# ChemComm



### **HIGHLIGHT**



Cite this: Chem. Commun., 2025, **61**, 12232

Received 12th June 2025. Accepted 9th July 2025

DOI: 10.1039/d5cc03327f

rsc li/chemcomm

# Tailoring defects and interfaces in sulfide solid electrolytes for high-performance solid-state sodium batteries

This review focuses on defect chemistry and ion transport in sodium sulfide solid electrolytes, emphasizing the influence of intrinsic and extrinsic defects, grain boundaries, and insights from advanced computational studies. By comparing sodium and lithium electrolyte systems, it highlights the unique challenges and opportunities in sodium-based solid electrolytes. Additionally, doping strategies, emerging materials, and hybrid approaches to enhance ionic conductivity and interfacial stability are explored. Practical implications regarding defect formation energies, grain boundary contributions, and interface effects are critically discussed, providing a comprehensive roadmap for advancing solid-state sodium batteries

### 1. Introduction

Clean and renewable energy sources are currently gaining attraction due to their ability to reduce greenhouse gas emissions, combat climate change, and provide sustainable, costeffective energy with less environmental impact. However, such greener energies need to be stored either for a shorter or longer duration before being used in practical applications. Among various energy storage technologies, lithium-ion batteries dominate the energy storage market due to their higher energy density, efficiency and longer cycle life. Due to concerns such as limited raw material availability (e.g., lithium and cobalt), the environmental impact of mining, higher costs and safety issues (fire risk), a more cost-effective alternative is imminent.<sup>2</sup> Also, the uneven global distribution of critical raw materials and a need for greener alternatives are key drivers for all-solid-state sodium batteries (ASSSBs). A wide distribution of sodium raw materials and abundance contribute to its lower cost than lithium counterparts. Sodium-ion batteries are further enabled for large-scale energy storage applications by solid electrolytes for safety and their ability to operate at higher temperatures with reduced material costs and improved stability.3 Unlike liquid-based batteries, the use of metallic sodium anodes plays a key role by offering high theoretical capacity and low redox potential, which enhances energy density significantly, while

Since the early report<sup>3</sup> of β-alumina as an electrolyte for sodium-sulfur batteries in 1960, various sodium ionconducting solid electrolytes have been explored since then. Among various solid-electrolytes, oxide, sulfides, halides, halides, and polymer electrolytes9 are the mostly commonly studied categories due to their physical and chemical properties such as high ionic conductivity, chemical and thermal stability, compatibility with sodium anodes, material abundance, and their potential for scalability. Despite these advantages, various ground-level problems such as poor ionic conductivity at room temperature, poor interfacial compatibility with electrodes, brittleness (for ceramics), air sensitivity (for sulfides), and limited mechanical stability in long-term cycling are hampering their commercial deployment for a long time. Other problems such as dendrite formation, high processing costs, limited electrochemical stability window, and sensitivity to air and moisture are also obstacles to their application in solidstate batteries. Therefore, to advance the true potential of ASSSBs for practical applications, this comprehensive review of the various modifications made to electrolyte materials to enhance their performance in meeting application demands is essential. Moreover, understanding grain boundary effects and interfacial stability between electrodes and sulfide electrolytes is also essential for fully harnessing the potential of sodium solid-state batteries, in conjunction with bulk defect engineering. Due to the complex nature of defects and ion transport phenomena, advanced computational techniques - such as density functional theory (DFT), ab initio molecular dynamics (AIMD), and emerging machine learning (ML) methods - have

their compatibility with solid electrolytes improves safety and cycle life in solid-state sodium batteries by multiple folds.

<sup>&</sup>lt;sup>a</sup> Department of Chemical Engineering, Hanyang University, Seoul 04763, Republic of Korea. E-mail: dongwonkim@hanyang.ac.kr

<sup>&</sup>lt;sup>b</sup> Department of Battery Engineering, Hanyang University, Seoul 04763, Republic of Korea

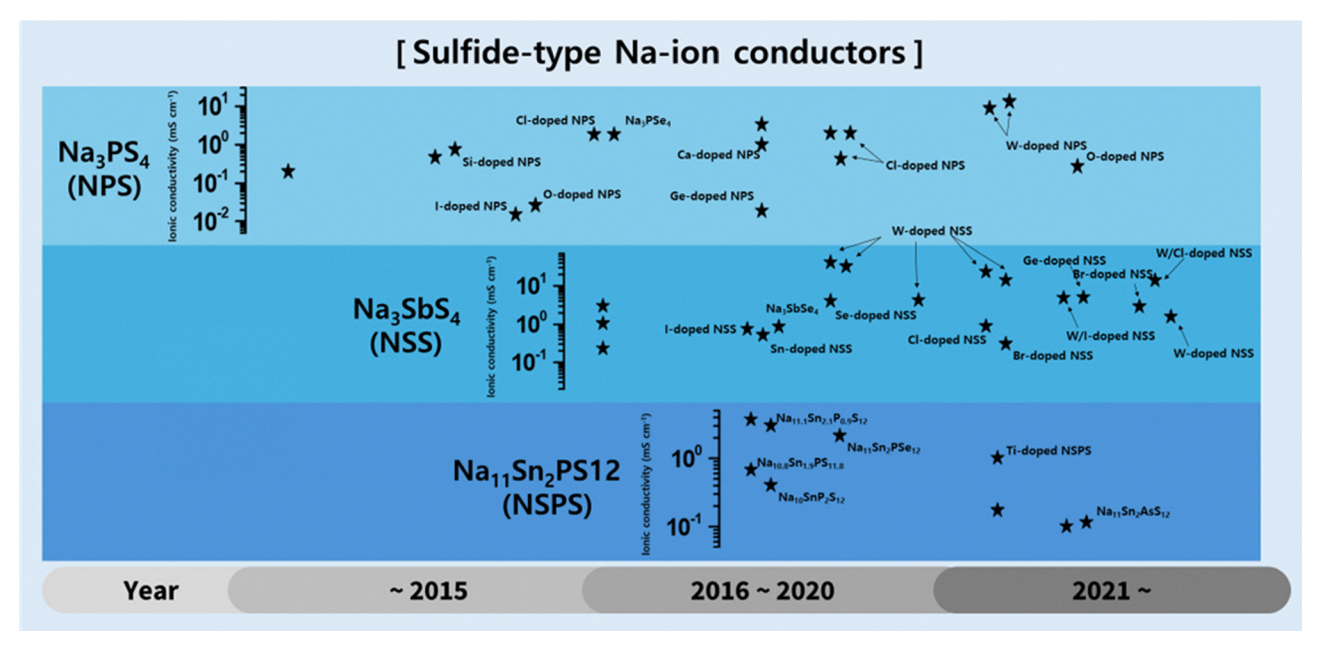


Fig. 1 Advancement history of representative sulfide-based Na-ion conductors with their doping chemistry.

become indispensable tools for predicting defect formation, ion migration pathways, and interfacial reactions. These computational approaches complement experimental techniques and help guide the optimization of materials through targeted defect and doping engineering.

After an inspiring report in 2012 by Hayashi et al.9 on Na3PS4 glass-ceramic super-ionic conductors with impressive ionic conductivity, sulfide-type Na-ion conductors started to gain serious attention from the scientific community (e.g. Fig. 1 represents the evolutionary history of sulfide-based Na-ion conductors). Building on previous research on Na<sub>3</sub>SbS<sub>4</sub>, where antimony replaces phosphorus, and other new sulfur chemistries like Na<sub>4</sub>MS<sub>4</sub> (M = Si, Sn, and Group IVA elements), Na<sub>11</sub>SnPS<sub>12</sub> has also been investigated and reported to exhibit impressive sodium-ion conductivities. In particular, among Na<sub>4</sub>MS<sub>4</sub>, candidates with structural modifications by doping or substitution display enhanced ionic conductivity compared with their parent chemistry. 10 For example, in Na<sub>4</sub>SnS<sub>4</sub>, when Sn is partially substituted by Si<sup>11</sup> a new 3D diffusion pathway is created, yielding a higher ionic conductivity of 1.6 mS cm<sup>-1</sup>. Another class of sulfide solid electrolytes with group IIIA elements, such as Ga and B are currently gaining attraction. In particular, B being an electrochemically inert element, is used as a passivating interlayer<sup>12</sup> at the electrode-electrolyte interface for enhancing interfacial stability and longer cyclability. Overall, Na<sub>3</sub>PS<sub>4</sub> (NPS), Na<sub>3</sub>SbS<sub>4</sub> (NSS), and Na<sub>11</sub>SnPS<sub>12</sub> (NSPS) are among the most extensively studied candidates within sulfide-based sodium solid electrolytes. Though a recent report<sup>13</sup> by Wang et al. discusses various broad aspects of this sulfide solid electrolyte, we particularly focus on the defect chemistry perspective and the corresponding effect on physical and chemical properties of the corresponding microstructures.

This review focuses on how defect chemistry (vacancies, dopants, and grain boundaries) affects the ionic conductivity and performance of solid electrolytes. To address the factors mentioned above, the following sections will discuss the roles of parameters such as defects and vacancies, grain boundaries, and defect formation energies for solid electrolytes. Following discussions, the impact of those tweaks on the overall performance of electrolytes and full cells is discussed briefly. Finally, some potential applications for sodium solid-electrolytes and required research directions for the future are also discussed.

### 2. Fundamental principles of defect formation

A crystalline solid is defined as a perfect crystal of solid, in which atoms are arranged in perfect order of a threedimensional periodic array. The term imperfection means any deviation from a perfect homogenous crystal lattice. In many physical processes in solids, such imperfections are essential including luminescence, atomic diffusion, crystal growth, and various deformations. In this chapter, we thoroughly discuss the various sources, causes and effects of such imperfections. Let us consider a layered oxide ABO2 composed of equal numbers of A and B metal atoms. The oxide compound is said to be ordered if the A and B atoms are arranged in a regular periodic arrangement with respect to one another. These periodically arranged A and B in 2D space form a lattice plane and each atom corresponds to lattice points. In thermal equilibrium, there may exist a crystal with a number of vacant lattice points up to an order of 2% near the melting point. If the removed ion from the vacancy is squeezed in between normal ions, into an interstitial position in the lattice, then we have a

Frenkel defect. Instead, if the removed ion is placed on the surface, we have a Schottky defect. These intrinsic defects are particularly critical in sodium sulfide solid electrolytes, as they directly influence sodium-ion mobility and overall ionic conductivity.

### Intrinsic defects such as vacancies

In 1926, Frenkel proposed the idea of point defects in crystals and explained their relationship with ionic conductivity in crystalline solids. He proposed that volume ionic conductivity occurs by the motion of positive or negative ions in the lattice under the influence of an electric field. In a perfect crystal, to achieve high ionic conductivity, imperfections such as vacant lattice sites or interstitial atoms would need to be created. Additionally, a great deal of energy is required to displace an ion from its lattice position. To overcome this difficulty, Frenkel proposed that point defects existed in the crystal lattices prior to the application of the electric field. These point defects led to the idea of non-stoichiometric compounds for e.g. let MX be a compound and there are possibilities of M > X or X > M. The solid overall must be neutral and if X > M there are M vacancies or for example cation vacancies. To compensate for charge, other defects must be present, and this phenomenon is commonly observed in solid-state electrolyte materials.

#### Extrinsic defects such as aliovalent doping

Point defects can be induced by impurity atoms, too. In sodium-based electrolytes, these impurity atoms typically occupy lattice sites or interstitial positions, modifying defect structures and significantly altering sodium-ion conduction pathways. For example, aliovalent doping with elements such as Si, Sn, or W in Na<sub>3</sub>PS<sub>4</sub> and Na<sub>3</sub>SbS<sub>4</sub> creates sodium vacancies or interstitials, thus enhancing ionic conductivity dramatically. Typically, these impurity atoms are not randomly arranged and some degree of clustering or ordering region often occurs, leading to linear, planar, and volumetric defects. Theoretically, the shear strength of perfect crystals is significantly higher than the actual shear strength observed in very pure crystals. This discrepancy has led many researchers to suggest that imperfections in real crystals are the primary reason for their lower strength. Normally, the atoms or ions are not in their normal position during dislocation and causes slip plane and permanent deformation by shear since they are not in their normal positions. With these fundamental principles established, the following sections will provide a detailed discussion on how intrinsic and extrinsic defects specifically manifest in sodium sulfide solid electrolytes and how they can be engineered to optimize ionic conduction.

### 3. Intrinsic and extrinsic defects in Na ion conductors

To begin with, Na<sub>3</sub>PS<sub>4</sub> is shown to coexist both in a glassy state (amorphous) and a glass-ceramic state upon a mechanochemical synthesis method by using a mixture of Na2S and P2S5.

Initially, Na<sub>3</sub>PS<sub>4</sub> was believed to exist in two polymorphs - a tetragonal phase with P421c space group and a cubic phase with a space group of  $I43m^{9,14-16}$  (Fig. 2(a) and (d)). While Na ions occupy the Na(6b) site in between PS<sub>4</sub><sup>3-</sup> tetrahedra of the bcc sublattice, in tetrahedra form this 6b site splits into two distinct sites [Na(2a) and Na(4d)] due to slight rotation of the PS<sub>4</sub><sup>3-</sup> polyhedral<sup>17</sup> and thus changing the lattice constants. In addition to these two phases, an additional orthorhombic phase with space group Fddd was also observed 18,19 when heated beyond 500 °C, characterized by notable changes in both the PS<sub>4</sub><sup>3-</sup> bonding and an abrupt increase in unit-cell volume increase. The transition of Na<sub>3</sub>PS<sub>4</sub> from cubic (at 270 °C) to a tetragonal phase at 420 °C has been evidently captured by in situ TEM analyses, 20 strongly correlating phase changes with the annealing temperature.21 Among both forms, the glassceramic form exhibits a notably higher ionic conductivity of about 0.2-0.46 mS cm<sup>-1</sup> at RT,<sup>22</sup> which attracted significant interest in this class of ion conductors. Theoretically, both cubic and tetragonal stoichiometric phases have similar low ionic conductivities with activation energies of 0.19 vs. 0.20 eV, respectively.<sup>21</sup> However, in practicality glass-ceramic (amorphous) Na<sub>3</sub>PS<sub>4</sub> exhibits a higher ionic conductivity (0.2 mS cm<sup>-1</sup>) than the crystalline tetragonal phase (0.01 mS cm<sup>-1</sup>).9 This difference in ionic conductivity between experimental and theoretical values is mainly driven by local factors such as defect concentrations and micro-strain, rather than crystal structure alone. Various theoretical, in particular MD simulation studies,<sup>17,21</sup> have confirmed that introducing a Na vacancy can dramatically increase ionic conductivity, which is discussed in later sections (Fig. 3). For example, Na<sub>3</sub>PS<sub>4</sub>-pristine without defects could display maximum conductivities of  $\sim 0.2$  mS cm<sup>-1</sup>, <sup>23</sup> whereas upon introducing Na vacancies as in Na<sub>2,94</sub>PS<sub>4</sub> a significant increase in ionic conductivity (theoretically  $\sim 200.0$  mS cm<sup>-1</sup>) could be achieved without much change in the crystal structure. This significant improvement in conductivity highlights that defect chemistry, rather than the material phase, plays a crucial role in achieving high ionic transport in sodium solid electrolytes.

For a long time, researchers have extensively investigated doping both at anionic and cationic sites as a widely followed method to modify the crystal structure and induce defects in perfect crystal structures. Based on Na<sub>3</sub>PS<sub>4</sub> systems, both cation and anion substitution are more prevalent. In particular, partial substitution of P with group IVA elements such as Si, Ge, and Sn introduces extra Na content or Na interstitials, causing intrinsic defects to the system. For example, in a report by the Tatsumisago group,  $^{24}$  the addition of  $\sim 6$  mol% Si in Na<sub>3</sub>PS<sub>4</sub> glass ceramics (amorphous) boosts room temperature ionic conductivity by 3 times from 0.25 to 0.74 mS cm<sup>-1</sup>. In another work by Adams et al., 25 doping of group IVA elements (Ge, Ti, and Sn) on Na<sub>3</sub>PS<sub>4</sub> was systematically performed with levels up to x = 0.1 in  $Na_{3+x}M_xP_{1-x}S_4$ . With the increase in atomic radii of dopants in sequence (Si < Ge < Ti < Sn), the corresponding lattice volume was added. However, the corresponding average site decreased in reverse order with Sn doping appearing to be the most promising. Experimental analysis of

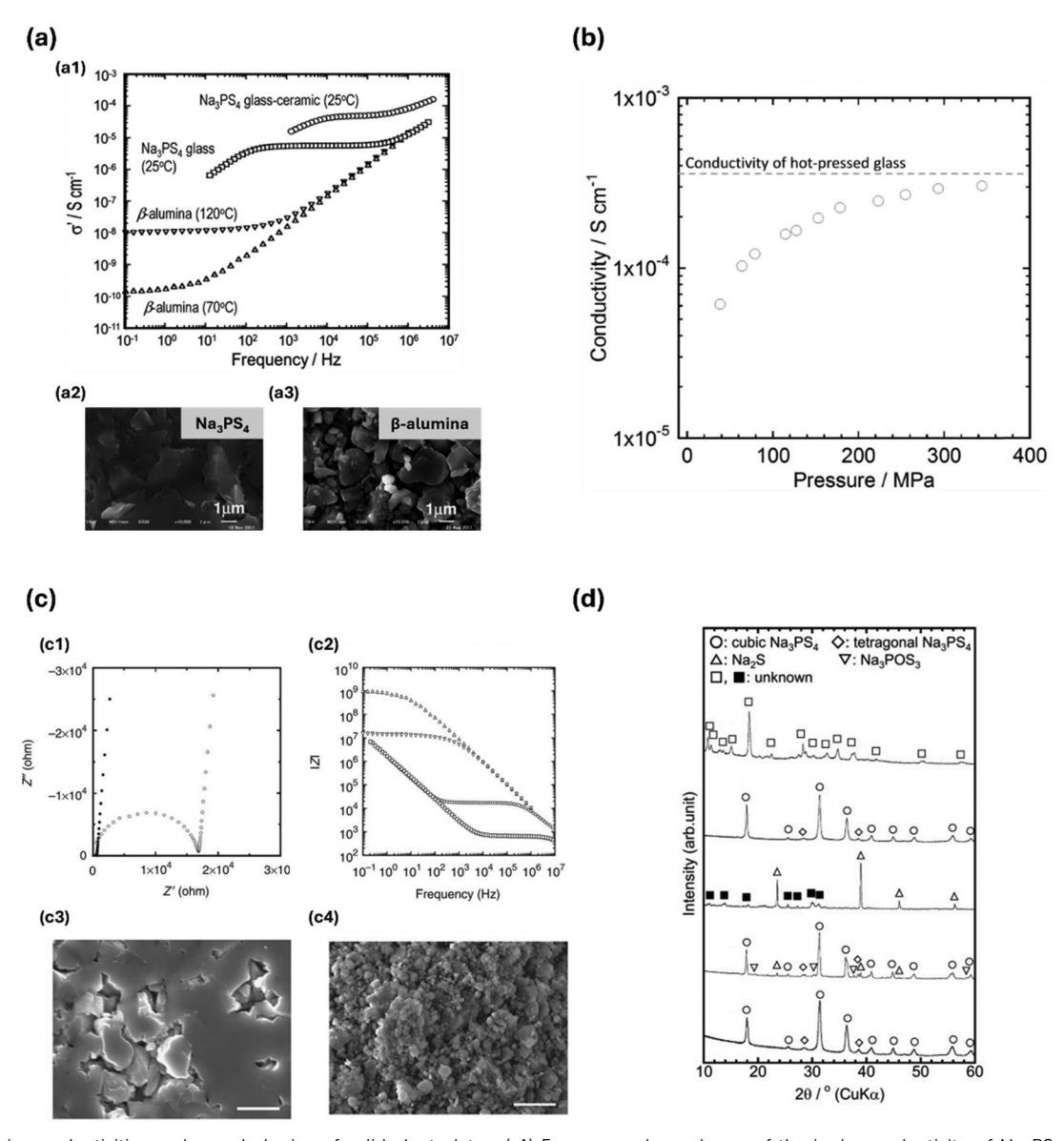


Fig. 2 (a) Ionic conductivities and morphologies of solid electrolytes. (a1) Frequency dependence of the ionic conductivity of Na<sub>3</sub>PS<sub>4</sub> glass, Na<sub>3</sub>PS<sub>4</sub> glass-ceramic, and β-alumina. Cross-sectional SEM images for the powder-compressed pellet. (a2) Na<sub>7</sub>PS<sub>4</sub> glass-ceramic and (a3) β-alumina. Reproduced with permission from ref. 5. Copyright 2014 The American Ceramic Society and Wiley Periodicals, Inc. (b) Ionic conductivities of 75Li<sub>2</sub>S-25P<sub>2</sub>S<sub>5</sub> depending on molding pressure. Reproduced with permission from ref. 6. Copyright 2016, The Author(s). (c) Ionic conductivities and morphologies of solid electrolytes.  $^9$  (c1) Impedance plots of the Na<sub>3</sub>PS<sub>4</sub> glass pellet (open circle) at 25  $^{\circ}$ C and the glass-ceramic pellet prepared at 270  $^{\circ}$ C (closed circle). (c2) Bode plots of the pellets of the Na<sub>3</sub>PS<sub>4</sub> glass (open circle, at 25 °C) and the Na<sub>3</sub>PS<sub>4</sub> glass-ceramic (open square, at 25 °C), and the  $\beta$ -alumina (open triangle (at 70 °C) and open reverse-triangle (at 120 °C)). Cross-sectional SEM images of (c3) the Na<sub>3</sub>PS<sub>4</sub> glass-ceramic pellet and (c4) the β-alumina pellet. Proposition Reproduced with permission from ref. 9. Copyrights 2017. Elsevier B.V. (d) XRD patterns of Na<sub>3</sub>PS<sub>4</sub> electrolytes. The patterns of Na<sub>3</sub>PS<sub>4</sub> prepared using 1,2-dimethoxyethane and dried (d1) at room temperature and (d2) heated at 270 °C. The patterns of Na<sub>3</sub>PS<sub>4</sub> prepared using diethyl ether dried (d3) at room temperature and (d4) heated at 270 °C. (d5) The pattern of Na<sub>3</sub>PS<sub>4</sub> prepared by mechanical milling. <sup>7</sup> Reproduced with permission from ref. 7. Copyright 2012, Springer Nature.

the same further confirmed the theory by achieving the highest ionic conductivity of 0.25 mS  ${\rm cm}^{-1}$  at RT. Similarly, incorporating other dopants such as W or As<sup>15,26,27</sup> has significant and impactful increase in ionic conductivity by reaching a conductivity of about 13 mS cm<sup>-1</sup>. Not just limited to the P position, cation doping to replace Na+ by aliovalent doping such as Ca was also performed by the Jung group. 28 Replacing some Na<sup>+</sup> in Na<sub>3</sub>PS<sub>4</sub> with Ca (Na<sub>3-2x</sub>Ca<sub>x</sub>PS<sub>4</sub>) stabilizes the cubic phase at RT

and generates additional Na vacancies that improve ionic conduction up to 1 mS cm<sup>-1</sup> under optimal Ca content of x = 0.135, yielding a maximum ionic conductivity.

Much like cation substitution, anion substitution by aliovalent and isovalent anions was also performed. For aliovalent substitution, halogen substitution (such as F, Cl, Br, I)29-31 at anionic sites can create Na vacancies for charge compensation, dramatically enhancing ionic diffusivity and conductivity. For

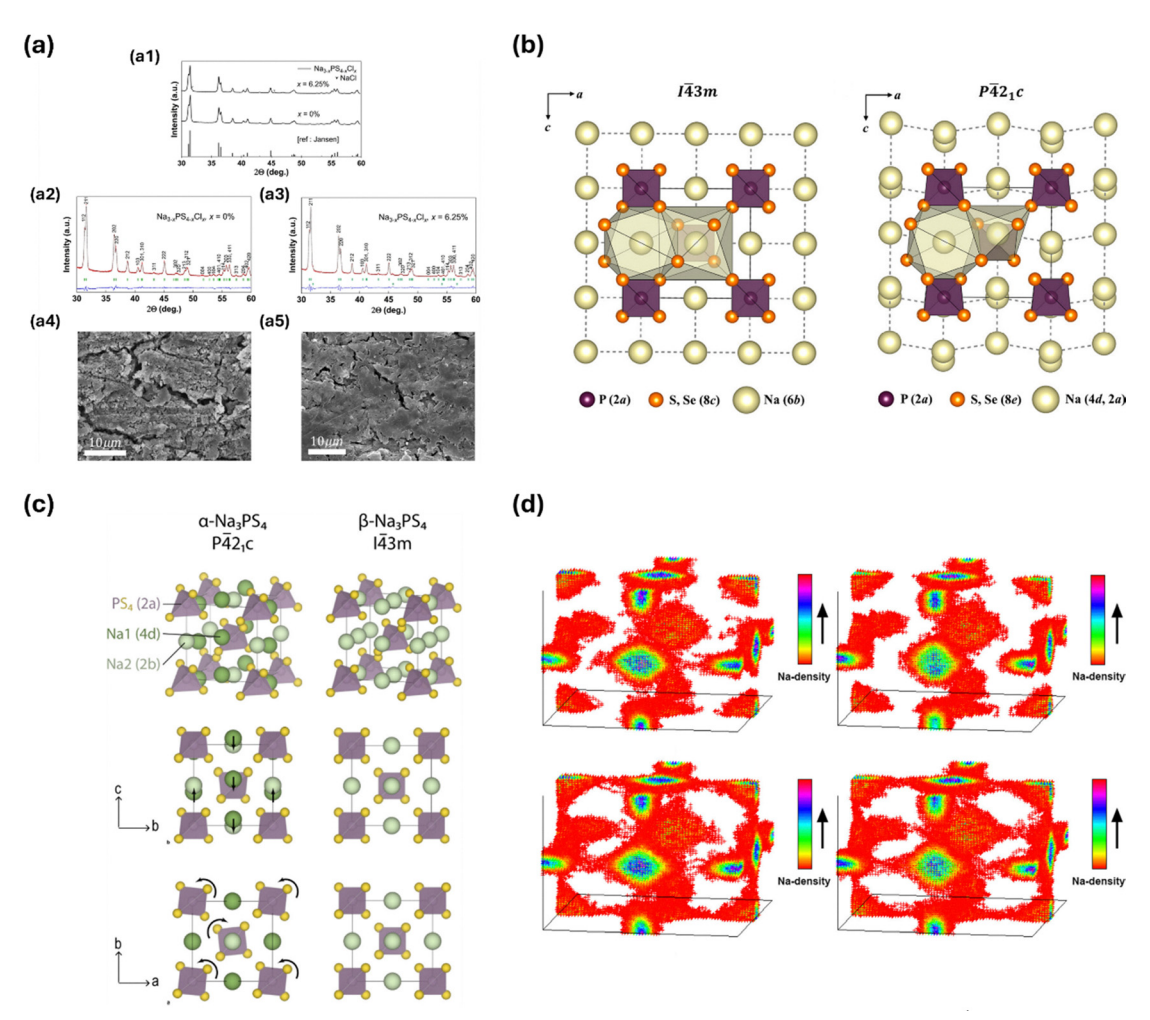


Fig. 3 (a) XRD patterns, refinement plot, and morphology of solid electrolytes.  $^{14}$  (a1) XRD patterns for t-Na<sub>3-x</sub>PS<sub>4-x</sub>Cl<sub>x</sub> with x = 0 and 6.25%. Refinement plot of (a2) the pristine t-Na<sub>3</sub>PS<sub>4</sub> and (a3) the Cl-doped t-Na<sub>3</sub>PS<sub>4</sub>. Solid red and black lines denote the observed and calculated XRD patterns, while the green ticks mark the position of the reflections allowed by the space groups of t-Na<sub>x</sub>PS<sub>4</sub> and NaCl. The difference between the observed and calculated patterns is signified by the blue line. SEM image of (a4) pristine t-Na<sub>3</sub>PS<sub>4</sub> and (a5) doped t-Na<sub>3-x</sub>PS<sub>4-x</sub>Cl<sub>x</sub> (x = 6.25%). Reproduced from ref. 14 under the terms of the Creative Commons CC BY license. (b) Cubic and tetragonal modification of  $Na_7PCh_4$  (Ch = S, Se),  $^{13}$  and the diffusion geometries for the preferred jump processes, shown along the (010) plane. In both polymorphs, the Na<sup>+</sup> ions go through a transition state that is only coordinated by the chalcogen anions, and the changing anion polarizability is expected to directly affect the interaction with the Na<sup>+</sup>. Reproduced with permission from ref. 13. Copyright © 2018, American Chemical Society. (c) Structural relationship between  $\alpha$  and  $\beta$ -Na<sub>3</sub>PS<sub>4</sub>. The transition occurs upon translation of the 4d Na1 atoms (highlighted in brown) and rotation of the PS<sub>4</sub> tetrahedra about the c-axis. The model for the  $\beta$ -phase shown here includes a single Na atom at the 6b position for simplicity, in contrast to the 1/4-occupied 24f site that results in slightly better fits of the Bragg diffractograms. 18 Reproduced with permission from ref. 18. Copyright 2021 Published by American Chemical Society. (d) Na-distribution during a 100 ps MD simulation<sup>17</sup> at 525 K for (d1) cubic Na<sub>3</sub>PS<sub>4</sub>, (d2) tetragonal Na<sub>3</sub>PS<sub>4</sub>, (d3) cubic Na<sub>2,94</sub>PS<sub>4</sub>, and (d4) tetragonal Na<sub>2,94</sub>PS<sub>4</sub>. Reproduced with permission from ref. 17. Copyright 2016 Published by American Chemical Society.

instance, Cl-doped t-Na $_3$ PS $_4$  can reach  $\sim 1.14$  mS cm $^{-1}$  at 30 °C, 14 while Br doping may provide ionic conductivities up to  $\sim 2.37$  mS cm<sup>-1</sup> at 300 K (Fig. 3(a)). However, a further increase in halogen doping may result in the formation of impurity phases that reduce ionic conductivity.32 Similar phenomena<sup>33</sup> were observed in other sulfide glasses such as Na<sub>3</sub>SbS<sub>4</sub> during processing at temperatures below at 200 °C in the presence of NaI to form an amorphous phase surrounding crystalline Na<sub>3</sub>SbS<sub>4</sub>. This 0.1NaI 0.9 Na<sub>3</sub>SbS<sub>4</sub> composite displayed double the ionic conductivity as high as 0.74 mS cm<sup>-1</sup>, highlighting the potential of sulfide solid-electrolytes for high-performance sodium-ion batteries. For iso-valent anion

substitutions, such as Se<sup>2-</sup> or O<sup>2-</sup>, the doping results in the softening of the lattice, lowering activation barriers and achieving room temperature ionic conductivities up to 0.11 mS cm<sup>-1</sup>, and modifies the lattice dynamics and helps in controlling the Na-ion conduction pathway. 16,34,35 Apart from experimental doping mechanisms, various theoretical simulations and predictions on addition of various other elements such as Ge and Sn are discussed in the theoretical studies section of this review. Given these significant improvements, to further optimize sulfide-based sodium-ion conductors, rational doping strategies remain a key research direction. In addition to enhancing bulk ionic conductivity, intrinsic and extrinsic

defect engineering may also influence grain boundary chemistry, potentially altering grain boundary resistance and interfacial stability, as explored in subsequent sections.

Similar to Na<sub>3</sub>PS<sub>4</sub>, Na<sub>3</sub>SbS<sub>4</sub> also exists in two polymorphs depending upon temperature. While the tetragonal phase (space group  $P2_1c$ ) is common at lower temperatures, <sup>36–38</sup> a cubic phase (space group 13m) is observed at hightemperatures. While the tetrahedra position consists of two SbS<sub>4</sub> tetrahedral units, with Sb on 2b sites and S on 8e sites, Na is positioned at a distorted octahedron (NaS<sub>6</sub>) and in a dodecahedron (NaS<sub>8</sub>)<sup>15</sup> with a 3D ion-diffusion network that spans both the a-b plane and along the c-axis. These distortions and Na vacancies at dodecahedron sites are the main reason for significantly enhanced Na-ion transport in Na<sub>3</sub>SbS<sub>4</sub> class conductors. Even under high pressure, the tetragonal structure of Na<sub>3</sub>SbS<sub>4</sub> was observed to be stable. On the cubic phase which typically appears at higher temperatures (300-350 °C), all Na sites are crystallographically equivalent.<sup>39</sup> However, cubicstructured Na<sub>3</sub>SbS<sub>4</sub> has been reported<sup>40-42</sup> to be stabilized at lower temperatures by the controlled synthesis method by preventing transition to the tetragonal phase at 150-180 °C. Between tetragonal and cubic phases, typically tetragonal Na<sub>3</sub>SbS<sub>4</sub> displays higher ion conductivity in the range of 1-3 mS cm<sup>-1</sup>, especially in dry synthesis<sup>37</sup> compared to 0.1-0.5 mS cm<sup>-1</sup> by the liquid phase method.<sup>33</sup> Irrespective of synthesis methods, Na vacancies are the crucial factor in enabling high ionic conductivity. Also, a planar network in the a-b plane formed by alternating NaS<sub>6</sub> and NaS<sub>8</sub> sites and interplane connections along the c-axis, where NaS<sub>6</sub> octahedra share edges, allowing Na<sup>+</sup> to hop between planes, emerges as a 3D transport pathway. 43,44 In comparison, tetragonal Na<sub>3</sub>SbS<sub>4</sub> typically shows an activation energy of about 0.22 eV, whereas cubic Na<sub>3</sub>SbS<sub>4</sub> exhibits a much lower activation energy, ranging from 0.036 to 0.06 eV in different studies necessitating stabilization of the cubic phase to reap significantly enhanced ionic conductivity. In addition to the above structural similarity, the research methodology adopted by various research groups is also very similar to Na<sub>3</sub>PS<sub>4</sub> counterparts such as in doping strategies and creating Na vacancies. In addition, some studies were aiming to stabilize phases, cumulatively sums up to efforts for enhancing ionic conductivity. Substitution of elements such as Ge<sup>45</sup> and Sn into Na<sub>3</sub>SbS<sub>4</sub> resulted in lattice expansion due to Na interstitials and boosting ionic conductivity by availing increased ion-diffusion pathways. Particularly in the case of Sn,46 the introduction of high Sn content leads to crystallization of the tetragonal phase (space group I4<sub>1</sub>/acd), indicating mixed Sb/Sn sites and multiple Na sites, all contributing to superior ionic conductivity. Among various dopants, stabilization of the cubic phase is best achieved by aliovalent W<sup>6+</sup> substitution. This resulted in some of the highest ionic conductivities exceeding 20 mS cm<sup>-1</sup> at RT, which is achieved by W<sup>6+</sup> substitution. The stabilization of the cubic phase is achieved by decreasing tetragonal distortion and with a bodycentered sublattice of SbS<sub>4</sub><sup>3-</sup> and WS<sub>4</sub><sup>2-</sup> units. 15,47 Depending on the doping level, the ionic conductivity also varied from 32 mS cm<sup>-1</sup> at RT for moderate doping levels  $x \approx 0.1$ –0.12 to

24.2 mS cm<sup>-1</sup> at RT for heavier doping ( $x \approx 0.3$ ) such as in  $Na_{2.895}Sb_{0.7}W_{0.3}S_4$  and drops further up to ~14.5 mS cm<sup>-1</sup> for a slightly orthorhombic variant. 48 Some studies 15,49 have indicated even higher ionic conductivities such as in Na<sub>2.9</sub>Sb<sub>0.9</sub>- $W_{0.1}S_4$  up to 41  $\pm$  8 mS cm<sup>-1</sup>. Overall, up to the moderate level of doping, with the W doping level rising the content of Na vacancies rises leading to a fall in activation barrier and increase in ionic conductivity. 47,48,50 In addition to single cation doping, co-doping strategies were also tried by the Sohn et al. group with additional cations such as Si4+ to increase vacancy formation and stabilize the conductive phase, resulting in ionic conductivity up to 20.2 mS cm<sup>-1</sup> at RT.<sup>51</sup> It is often for glass-ceramic approaches and solution-based syntheses to yield high ionic conductivity often surpassing 4-5 mS cm<sup>-1</sup> at RT.<sup>52</sup> Overall, cation doping in Na<sub>3</sub>SbS<sub>4</sub> especially with W<sup>6+</sup> has proven highly effective for generating Na vacancies, enlarging the lattice, and stabilizing more isotropic cubic or near-cubic frameworks, ultimately delivering some of the highest ionic conductivities reported for sulfidebased sodium solid electrolytes.

On the other hand, doping at anionic sites such as Se<sup>2-</sup> or halogens is also performed by various research groups. In a study by Yao et al., S<sup>2-</sup> anions are replaced by larger Se<sup>2-</sup> ions systematically to expand the lattice<sup>53</sup> and to induce tetragonal to cubic phase transitions.<sup>54</sup> For example, Na<sub>3</sub>SbS<sub>3</sub>Se, Na<sub>3</sub>SbS<sub>2</sub>Se<sub>2</sub>, and Na<sub>3</sub>SbSSe<sub>3</sub> adopt a cubic structure, whereas undoped Na<sub>3</sub>SbS<sub>4</sub> is tetragonal. In this study,<sup>54</sup> the varying Se content displayed varied ionic conductivities but similar activities. Not just limited to Se content, synthesis methods also significantly affect ionic conductivity as demonstrated in liquid-solid fused synthesis, which demonstrated higher ionic conductivity up to 4.03 mS cm<sup>-1</sup> compared to purely liquid or solid-state routes. 53-55 On halogen doping, few structural modifications happen as Cl doping can slightly elongate the a-axis while shortening the c-axis, reducing tetragonal distortion.<sup>56</sup> In Br doping, similar lattice volume expansion happens but retains the tetragonal framework at moderate doping.<sup>57</sup> In contrast to these, in I- doping if dopant levels are too high, an impurity phase (e.g. NaI) is formed as mentioned earlier.<sup>33</sup> In terms of ionic conductivity, Cl<sup>-</sup> doped Na<sub>2,95</sub>SbS<sub>3,95</sub>Cl<sub>0.05</sub> ~ 0.9 mS cm<sup>-1</sup>, while Br doping Na<sub>2.76</sub>SbS<sub>3.76</sub>Br<sub>0.24</sub> exhibits about 0.31 mS cm<sup>-1</sup>. Unlike in Cl or Br, a composite of 0.1 NaI-0.9 Na<sub>3</sub>SbS<sub>4</sub> boosts ionic conductivity from 0.34 mS cm<sup>-1</sup> (undoped) to  $0.74 \text{ mS cm}^{-1}$ . When using the aqueous approach for synthesis, RT ionic conductivity also increased with an increase in Cl concentration (0  $\leq x \leq 0.15$ ) and similar concentration studies were performed using Br in the anionic site. 57,58 Overall, halogen doping typically creates Na vacancies for charge balance and slightly distorts the lattice, thus facilitating faster Na<sup>+</sup> ion transportation.

Unlike  $Na_3PS_4$  and  $Na_3SbS_4$  which share some similarities,  $Na_{11}Sn_2PS_{12}$  is another sulfide solid electrolyte type and class on its own following the roots of  $Li_{10}GeP_2S_{12}$  (LGPS) ionic conductors.<sup>59–63</sup> However, like its previous counterparts, the ionic conductivity of tetragonal  $Na_{11}Sn_2PS_{12}$  has also undergone significant improvement and fine tuning by introducing

various dopants/substitutions at both cationic and anionic sites. In contrast to previous systems upon cation substitution (Sb<sup>5+</sup>) at the P site, expansion in unit cell was observed for Na<sub>11</sub>Sn<sub>2</sub>SbS<sub>12</sub> but ionic conductivity dropped to 0.56 mS cm<sup>-1</sup> from 1.4 mS cm<sup>-1</sup> for the undoped system due to stronger Na-S bonding and altered Na<sup>+</sup> site occupancy. 64,65 In another study,66 simultaneous doping both at cationic and anionic sites resulted in enhancement of ionic conductivity up to  $\sim 0.66$  mS cm<sup>-1</sup>. Apart from Sb, other group IVA dopants such as Si<sup>4+</sup>, Ge<sup>4+</sup>, and Sn<sup>4+</sup> can also modify vacancy concentrations, influencing the balance between Na<sup>+</sup> diffusion pathways and "excess vacancies" that might hinder Na conduction later. For example, in a study by Yao et al., Si substitution in  $Na_{11,25}Sn_{1.5}P_{0.75}Si_{0.75}S_{12}$  achieves an ionic conductivity of 1.6 mS cm<sup>-1</sup> and similar studies with Ge or Sn reveal that ion-transport activation energy decreases if the vacancy concentration is optimized upto a sharp peak value. 67-69 Upon anion substitutions such as Se<sup>2-</sup> for S<sup>2-</sup>, lattice parameters widen while preserving the tetragonal structure due to strong Na-S bonding as discussed earlier. 64,66,70 This change in lattice parameters results in ionic conductivity of 3.0 mS cm<sup>-1</sup> slightly lower than pristine 3.7 mS cm<sup>-1</sup> but exhibits a smaller activation energy.<sup>71</sup> Equivalent results are observed in another independent study displaying ionic conductivity of 2.15 mS cm<sup>-1</sup> and lower Na-Sn/Na-Se bonding energies, supporting 3D Na<sup>+</sup> conduction pathways. 70 These conductivity values put this class of ionic conductors in an emerging category next to the Na<sub>3</sub>PS<sub>4</sub> and Na<sub>3</sub>SbS<sub>4</sub> group of ionic conductors.

### 4. Grain boundary and interfacial effects

In addition to defects and vacancies that lead to an increase in ionic conductivity, which determine the overall cell performance of batteries; there is another critical factor such as grain boundary and interfacial stability of electrolytes towards electrodes that also determines the electrochemical performance of batteries.<sup>58</sup> The interfacial compatibility between metallic Na anode and sulfide solid electrolyte strongly influences the Na dendrite formation and growth, strongly influencing the cycling stability of solid-state Na batteries. Among various solid-electrolytes, sulfide-based electrolytes are known to show narrower electrochemical windows, as indicated in various first-principle calculations.72-74 To enhance the electrochemical stability, various strategies such as surface treatment, modifications, and artificial interlayers at the interface were fabricated, which are discussed in later sections as stabilization strategies. Grain boundary and interfacial effects in sodium sulfide electrolytes are inherently influenced by local defect structures, including vacancy concentrations, dopant segregation, and structural disorder. These defect-driven phenomena can significantly alter ion migration kinetics and interface stability, directly affecting overall electrochemical performance.

To begin with, interfacial stability between Na anodes and sulfide ion conductors is discussed here. Na metal anodes are

considered as ultimate anodes due to their higher energy density and being lighter in weight compared to many other complex anodes (e.g. alloy type anodes such as MoS<sub>2</sub>). However, the greater disadvantage of metallic Na is its high reactivity, leading to decomposition of sulfide solid electrolytes at the interface. Many experimental<sup>75,76</sup> and theoretical studies (such as DFT calculations) including a study by Ceder et al.<sup>58</sup> have validated that Na<sub>2</sub>PS<sub>4</sub> can decompose into Na<sub>2</sub>S and Na<sub>2</sub>P below  $\sim 1.55 \text{ V} \text{ vs. Na/Na}^+$ . Similar reactions at the Na<sub>3</sub>SbS<sub>4</sub>/Na interface are also found to produce Na2S and Na3Sb, which acts as a protective layer. To mitigate this issue, many new alloy-based anodes such as Na-In and Na-Sn alloys have been found to vield stable interfaces with sulfide electrolytes long with reducing interfacial polarization and overpotential in symmetric cells. 77,78 In another study performed by Ong et al., halogen doping (Cl<sup>-</sup>) was performed on Na<sub>3</sub>PS<sub>4</sub> to form a NaCl passivating interface. 14,79 This "salting" effect creates an electroninsulting solid electrolyte interphase (SEI) and maintains Na+ transport, thus reducing further decomposition of the electrolyte. In the case of substituting  $S^{2-}$  anions by  $O^{2-}$  anions in Na<sub>3</sub>PS<sub>3</sub>O the reaction with Na metal was decelerated, thereby improving interfacial stability.80 In another study,81 interlayer formation and interfacial contact can be facilitated by applying the stack pressure on the symmetrical cells. Both the interfacial resistance and total resistance decreased with increase in stack pressure up to 100 MPa and remained unchanged thereafter.

To counteract the highly reactive Na metal, various stabilization strategies have been adopted by different research groups as mentioned earlier (Fig. 4). These strategies mainly fall into three main categories:

- (1) Treatment of sulfide conductors.
- (2) Modification on Na metal anodes.
- (3) Artificial interlayer at anode/electrolyte interfaces.

The above strategies are discussed concisely and not in detail to avoid deviation from the scope of this review article. Firstly, in the treatment of sulfide conductors, doping and compositional adjustments are performed in numerous studies. For example, Cl-doping in Na<sub>3</sub>SbS<sub>4</sub> or Na<sub>3</sub>PS<sub>4</sub> and Odoping in Na<sub>4</sub>P<sub>2</sub>S<sub>7</sub> (NaPS) can modify reaction pathways, forming more stable interfacial products.82 In another strategy, simple exposure to ambient air such as for Na<sub>3</sub>SbS<sub>4</sub> can form a thin hydrated layer, converting a mixed conducting interface into a protective, passivating film for stabilization.83 For surface modification of Na metal anodes, surface deposition of alucone84 or reacting Na with phosphorus sulfide (P4S16) can create a thin Na<sub>3</sub>PS<sub>4</sub> passivation film, 85 resulting in dendrite suppression and smoother plating/stripping profiles for ion conductors. Lastly, artificial interlayers such as polymeric interlayers and liquid/phase-transition interlayers act as interlayerblocking electron flow and enables extended plating/stripping cycles but only at moderate currents. For example, the cellulose-poly(ethylene oxide) (CPEO) interlayer blocks electron flow and stabilizes the Na/Na<sub>3</sub>SbS<sub>4</sub> interface.<sup>87</sup> Similar observations are seen in other studies involving an ionic liquid ((PYR/ Na)TFSI) interlayer and other phase-transition polymers. 86,87 Overall, these interface engineering approaches such as

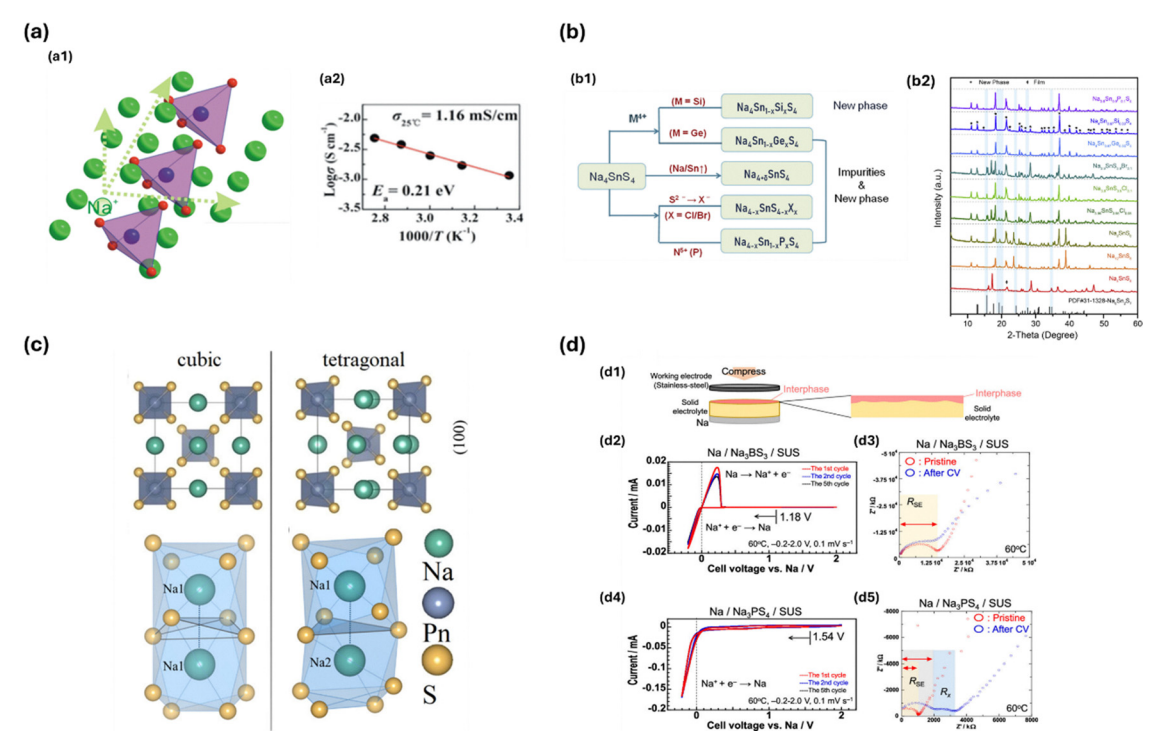


Fig. 4 (a) Crystal structure and ionic conductivities of  $Na_3PSe_4$ . (a1) Crystal structure and the sodium ion at the diffusion channels formed by PSe4 tetrahedra. (a2) Arrhenius conductivity plot of  $Na_3PSe_4$ . Reproduced with permission from ref. 10. Copyright 2015 Published by Wiley-VCH Verlag GmbH & Co. KGaA, Weinheim (b1) Design strategy<sup>11,12</sup> and (b2) X-ray diffraction patterns of the samples derived from  $Na_4SnS_4$ . Reproduced with permission from ref. 11. Copyright 2019 Published by Elsevier B.V. (c) Unit cells of the cubic and tetragonal  $Na_3PnS_4$  (Pn = P, Sb) and a full  $Na^+$  occupancy within the direct diffusion pathway found in both the polymorphs. Reproduced with permission from ref. 15. Copyright 2019 Published by American Chemical Society. (d) Formation of the interphase in  $Na_3BS_3$  glass and  $Na_3PS_4$  glass ceramic solid electrolytes by cyclic voltammetry. (d1) Schematic diagram of the cells and the interphases generated on solid electrolytes in contacting stainless steel as working electrodes. Cyclic voltammogram of the cells with (d2)  $Na_3BS_3$  glass and (d4)  $Na_3PS_4$  glass—ceramic at 60 °C. The scan rate was 0.1 mV s<sup>-1</sup> from -0.2 to 2.0 V. (d3) and (d5) Nyquist plots of each cell before and after cyclic voltammetry, respectively. The resistances of solid electrolytes and a newly developed component are denoted as  $R_{SE}$  and  $R_{XV}$  respectively. Reproduced with permission from ref. 12. Copyright 2016 Published by American Chemical Society.

electrolyte doping for protective layers on Na ion conductors or inserting a specialized interlayer help to minimize decomposition, prevent dendrite growth, and enhance the cycling performance of sulfide-based solid electrolytes and enable employing them in solid-state Na batteries.

Compared to interfacial effects, grain boundaries have lesser impacts particularly on sulfide solid electrolytes. In oxidebased solid electrolytes, grain boundaries are generally regarded as an ion transport barrier, hindering ion conduction significantly.21,88 However, grain boundaries were found to have a lesser impact<sup>89,90</sup> or be less clear in the sulfide electrolytes due to contradicting results from numerous studies. For example, in some studies, grain boundaries were found to have an impeding effect, 9,21,88 whereas another study suggested little to no effect on overall ionic conductivity (Fig. 2(c)). Other than ion transport, grain boundaries also have additional roles in dendrite formation and defect segregation. 91-94 However, the interplay between nano-crystallites and grain boundaries is not fully understood and prompts further investigation. 95,96 In the case of Na<sub>3</sub>PS<sub>4</sub>, while some reports (e.g. Krauskopf et al. 89) suggest minimal grain boundary resistance in these "mechanically soft" sulfides, other studies have proposed otherwise. To understand

further, on comparing with lithium counterparts<sup>88,97,98</sup> similar trends and variations are observed suggesting variability in the effect of grain boundaries from case to case. Such ambiguity suggests the need for deeper investigations into grain boundary behavior in sulfide-based solid electrolytes, particularly regarding whether and how grain boundaries facilitate or hinder ion transport in these materials—an issue that merits a dedicated review in its own right. Given these ambiguities, systematic computational and experimental investigations explicitly targeting defect segregation and chemistry at grain boundaries are essential to better understand and potentially exploit these phenomena in sodium-based sulfide electrolytes.

# 5. Advanced computational and experimental techniques

Advanced computational methods such as density functional theory (DFT), *ab initio* molecular dynamics (AIMD), and emerging machine learning (ML) approaches have significantly deepened the understanding of defect chemistry, ion transport mechanisms, and interfacial phenomena in sodium sulfide

solid electrolytes. As discussed in an earlier section, existence of defects, low energy barrier for Na ion migration, and high concentration of mobile carriers are prerequisites to obtaining high diffusivity in ion conductors. 99 Though various critical challenges that need to be overcome have stacked up, only a handful of processable Na-ion conductors with high ionic conductivities have been reported and experimentally validated. To address this knowledge gap, various research groups have simulated or predicted different chemistries to understand doping effects and Na vacancies. First-principles calculations have been performed on Na-based sulfide solid electrolytes to understand the diffusion mechanism as well as many novel Na-ion conductors with new compositions and structures. 17,100 To begin with, in a study on Na<sub>3</sub>PS<sub>4</sub> with both experimental and simulation techniques, Delaire et al. 101 combined quasi-elastic neutron scattering (QENS) experiments and ab initio molecular dynamics (AIMD) simulations to study the atomic dynamics in Na<sub>3</sub>PS<sub>4</sub>. These studies were performed in a wide temperature range of 100-600 K and as a result, temperature evolution of QENS spectra and fitted results showed that the estimated Na-ion jump length is 3.6 Å and the diffusion coefficient at 600 K is in the of order 10<sup>-6</sup> cm<sup>2</sup> s<sup>-1</sup> (Fig. 3(d)). Additionally, the ionic conductivity of tetragonal Na<sub>3</sub>PS<sub>4</sub> could be increased by ten times due to a consolidated mechanism by applying external pressure. 49 In another first principle investigation by Zhu *et al.*,  $^{100}$  RT ionic conductivities of 1.66  $\times$  10<sup>-3</sup> and 1.07 imes 10 $^{-2}$  S cm $^{-1}$  were achieved by 6.25 mol% Si and 6.25 mol% Sn-doped cubic Na<sub>3</sub>PS<sub>4</sub>, respectively. Even upon similar molar % doping of both Sn and Si, the enhanced ionic conductivity by the Si counterpart is attributed to excess Na<sup>+</sup> ions occupancy in the interstitial Na2 site and promoting faster ionic transport. In many cases, high sodium conductivity is activated once vacancies or interstitials are introduced into the structure through P cation or S anion aliovalent doping. 17,100,102,103 A first-principles computation by Ong et al., successfully predicted that 6.25% doping of Si<sup>4+</sup> for P<sup>5+</sup> in C-Na<sub>3</sub>PS<sub>4</sub> with interstitials can achieve ionic conductivities >10<sup>-3</sup> S cm<sup>-1</sup> at RT, which was validated by experimental results too. 100 In 2019, Islam et al. studied the superior ionic conductivity of these ionic conductors from a grain boundaries perspective by applying a micro-scale simulation approach. 104 By using two model electrolyte systems of Na<sub>3</sub>PS<sub>4</sub> and Na<sub>3</sub>PO<sub>4</sub>, a study revealed higher grain boundary resistance for Na<sub>3</sub>PO<sub>4</sub>, decreasing ionic conductivity with decreasing grain volume. Additionally, evidence of over-coordination of Na ions at the grain boundaries was also observed. In a molecular dynamics simulation<sup>105</sup> by Yang et al., tetrahedral alignment and covalent bonding of isostructural counterparts Na<sub>3</sub>PS<sub>4</sub> and Na<sub>3</sub>VS<sub>4</sub> isolated tetrahedral units were studied. AIMD simulations show that Na<sup>+</sup> migrates far more effectively in type I structures, with lower activation energies ( $\sim 0.3$  eV for Na<sub>3</sub>PS<sub>4</sub>). In contrast, type II Na<sub>3</sub>VS<sub>4</sub> has the highest activation energy of 2.6 eV and minimal Na<sup>+</sup> diffusion, consistent with experiments showing extremely low conductivity.

After the unprecedented ion conductivity at RT (order of  $10^{-2}~S~cm^{-1}$ ) reported for W-doped Na $_3SbS_4$ , the conductivity

value in the composition Na<sub>2.88</sub>Sb<sub>0.88</sub>W<sub>0.12</sub>S<sub>4</sub> is found to be higher than its undoped phase in the order the same as its lithium counterparts. 15,47 Apart from high conductivity, NSS also exhibits remarkably good chemical stability vs. air/H2O, which is not common for other sulfide solid electrolytes. 36,38,106 The origin of this stability was explained on the basis of hard-soft acid-base theory. 47,107 In 2017, a simultaneous experimental and computational study by Holzwarth et al., 108 explored the tetragonal phase of NSS and its interphase with a metallic sodium anode. Its computer simulation inferred the likelihood of a relationship between NSS and its interface, which involved the conversion of tetrahedral SbS<sub>3</sub><sup>2-</sup> ions of the bulk electrolyte into trigonal pyramidal ions SbS<sub>3</sub><sup>2-</sup> at the interface. In an effort to understand the ion conduction mechanism and aliovalent cation dopant effects in Na<sub>3</sub>SbS<sub>4</sub>, Tateyama et al. conducted a first principle calculation study, 109 which showed that Na vacancies played a significant role in superionic conductivity. A comparison between the two dopants (Mo<sup>6+</sup> and W<sup>6+</sup>) revealed that the conductivity enhancement arises from two key factors: a reduction in Na<sup>+</sup> ion activation energy and an expansion of the Na Wyckoff cages of WS<sub>4</sub>/MoS<sub>4</sub> relative to the host SbS<sub>4</sub> volume.

For the Na<sub>11</sub>Sn<sub>2</sub>PS<sub>12</sub> system, Richards et al. utilized a computation-guided approach to discover and synthesize this Na<sub>10</sub>SnP<sub>2</sub>S<sub>12</sub>, which achieved performance on par with the bestknown sulfide solid electrolytes of that time. 110 The authors combined density-functional theory (DFT) predictions of phase stability, ionic diffusion from AIMD, and experimental validation to show that Na<sub>10</sub>SnP<sub>2</sub>S<sub>12</sub> has a room-temperature ionic conductivity of ~0.4 mS cm<sup>-1</sup> and an activation energy of  $\sim 0.35$  eV (Fig. 5(a)). Another study by Ramos et al. in 2018 investigated how sodium-ion mobility in sulfide solid electrolytes was governed by crystal structure and defect chemistry.<sup>65</sup> Specifically, the study compares two closely related materials, Na<sub>11</sub>Sn<sub>2</sub>PS<sub>12</sub> with a P center and Na<sub>11</sub>Sn<sub>2</sub>SbS<sub>12</sub> with a Sb center showing differences in the arrangement of Na sites and occupancy, thus influencing their ionic conductivity and stability. In this study it was confirmed that SB-based materials showed higher occupancy of Na in regular Na (1) and Na(2) sites and lower occupancy on interstitial Na(6) sites leading to vacancies. However, overall sodium mobility compared to the P-based material is low due to stronger Na-S binding and a slightly higher activation energy of  $\sim 0.34$  eV (vs.  $\sim 0.25$  eV). Exploiting similar benefits of Na vacancies and quicker 3D Na-ion conduction pathways, Wang et al. 111 proposed a Na<sub>10.8</sub>Sn<sub>1.9</sub>PS<sub>11.8</sub> with ionic conductivity up to 0.67 mS cm<sup>-1</sup> at RT. Though previously predicted Li<sub>10</sub>GeP<sub>2</sub>S<sub>12</sub>-type (LGPS) "Na<sub>10</sub>SnP<sub>2</sub>S<sub>12</sub>" is prone to be structurally unstable, this newly reported composition gains extra stability from its higher Navacancy content. Therefore, these advanced computational predictions, combined with targeted experimental validations, serve as powerful tools in defect engineering and optimizing material properties, thereby enabling informed designs of high-performance sulfide electrolytes for sodium solid-state batteries.

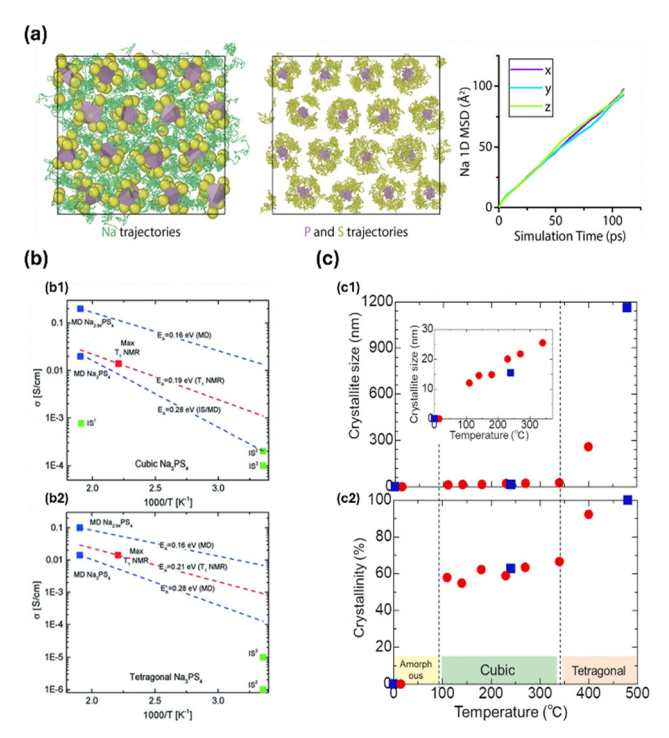


Fig. 5 (a) Atomic mobility results from ab initio molecular dynamics of  $\gamma$ -Na<sub>3</sub>PS<sub>4</sub>. Atomic trajectories of (a1) Na and (a2) P and S (green, purple and yellow lines, respectively) shown in projection through the bc plane for 50 ps after equilibration of a 900 K simulation without extrinsic vacancies. 131 (a3) Na<sup>+</sup> mean-squared displacements (MSD) in each spatial dimension. Reproduced with permission from ref. 131. Copyright 2021, Published by Elsevier B.V. (b) Comparison of conductivities for (b1) cubic Na<sub>3</sub>PS<sub>4</sub> and (b2) tetragonal Na<sub>3</sub>PS<sub>4</sub>. Indicated are the conductivities obtained by impedance spectroscopy, solid state NMR T1 relaxation and MD simulations (MD).<sup>21</sup> Reproduced with permission from ref. 21. Copyright 2016, Published by The Royal Society of Chemistry. (c) Temperature dependence of (c1) crystallite size and (c2) crystallinity.<sup>20</sup> Reproduced with permission from ref. 20. Copyright 2019, published by American Chemical Society.

## 6. Comparative analysis of sodium vs. lithium systems

In a periodic table, both lithium and sodium belong to the same alkali metal group 1 and exhibit almost similar chemical properties due to the isoelectronic configuration. While most of the fundamental principles governing ionic mobility and stability are comparable, due to bigger ionic radii, electronegativity and abundance differences, sodium systems present a unique set of challenges and opportunities. Before comparing lithium vs. sodium systems for ion-conducting electrolytes, it is right to acknowledge that sodium ion conductors irrespective of their chemistries trace their roots from Li counterparts, as shown in Table 1. In 2012, Hayashi et al. developed the cubic Na<sub>3</sub>PS<sub>4</sub> inspired by Li<sup>+</sup> ion conducting electrolyte made from the Li<sub>2</sub>S-P<sub>2</sub>S<sub>5</sub> system, <sup>6,9,96</sup> which exhibited high ionic conductivities and wide electrochemical stability window (Fig. 2(b)). Since then, many improvements have been made to Na systems and have always shadowed their lithium counterparts such as Si and Se<sup>10,24</sup> substitutions, which led to the prediction of Na<sub>3</sub>SbS<sub>4</sub> in late 2015 by Ceder et al. 112 In the same year, inspired by the record high ionic conductivity of Li<sub>10</sub>GeP<sub>2</sub>S<sub>12</sub> (LGPS), 113 the existence of isostructural Na counterpart  $Na_{10}MP_2S_{12}$  (M = Si, Ge, Sn) was predicted by first principle calculations as a metastable state by Kandagal et al.60 On comparison, LGPS displayed room temperature ionic conductivities of about 12 mS cm<sup>-1</sup>, whereas NGPS was predicted to be 1/3 of it up to 4.7 mS cm<sup>-1</sup>, which was higher than any other Na-ion solid electrolytes for Na-S batteries. In later stages, Richard et al. expanded  $Na_{10}MP_2S_{12}$  to phases with M = Si or Sn. 110 In 2017, another independent study by Tsuji et al. synthesized NGPS and found its room temperature Na<sup>+</sup> ion conductivity to be 0.012 mS cm<sup>-1</sup>, which is about 300 times lower than predicted earlier. Parallelly, doping/substitution at anionic sites was performed by some research groups to enhance ionic diffusivity compared with in cation substitutions. Following Se substitution in lithium sulfides, 60,114 enhancing ionic conductivity in comparison with their pristine compounds, the same approach was followed to develop Na<sub>3</sub>PSe<sub>4</sub> and evaluate its ionic conductivity<sup>10</sup> (Fig. 3). In a study by Ong et al. studying the role of Na+ interstitials and dopants, 100 aliovalent doping of M4+ for P5+ was as discussed in an earlier section. One interesting finding was that the Sn doped structure has a slightly larger channel size and free channel volume than the Si-doped structure. However, the trend was the opposite in  $Li_{10}MP_2S_{12}$  (M = Si, Ge, Sn)<sup>115</sup> with an Li<sup>+</sup> conductivity of Sn < Si. They speculated that the difference may have arrived due to the different dimensionality of diffusion between LMPS (Quasi 1D) and NMPS (3D) and different diffusing species Li<sup>+</sup> and Na<sup>+</sup>. These differences in ionic diffusion behavior can be fundamentally attributed to variations in defect formation energies, defect types, and defect-mediated ion migration pathways inherent to the structures of sodium and lithium sulfide electrolytes. In 2020, Yao et al. 116 studied new chemistries of the Na-Sb class with S and Se co-doped as anions exhibiting an ionic conductivity of 0.66 mS cm<sup>-1</sup>. Though the ionic conductivity was not on par, a unique bi-layer approach exhibited improved stability of sodium. Again, this strategy was also followed by LGPS counterparts in enhancing their electrolyte stability. Therefore, a deeper understanding of defect chemistry and defectmediated ion transport mechanisms is essential to fully exploit the similarities and differences between sodium and lithium sulfide electrolytes for targeted electrolyte optimization.

# 7. Emerging materials and hybrid strategies

Recent advances in sodium sulfide electrolytes largely rely on innovative defect engineering strategies, wherein doping and hybrid material approaches are employed to strategically manipulate defects for enhanced ionic conductivity and stability. From earlier discussions, it is evident that sulfide-based solid electrolytes have shown tremendous improvements in terms of their performance and enable safer all-solid-state sodium batteries supplemented by various

Table 1 Ionic conductivity comparison of sulfide sodium electrolytes and their lithium counterparts

	Sodium counterpart		Lithium counterpart		
Electrolyte family	Formula	Ionic conductivity (in mS cm <sup>-1</sup> )	Formula	Ionic conductivity (in mS cm <sup>-1</sup> )	Ref.
$\overline{A_3BS_4}$	Na <sub>3</sub> PS <sub>4</sub>	0.46	Li <sub>3</sub> PS <sub>4</sub>	0.164	22 and 117
$A_3BS_4$	$Na_3SbS_4$	1.0	Li <sub>3</sub> SbS <sub>4</sub>	0.0015	36 and 118
$A_{10+x}B_3S_{12}$	$Na_{11}Sn_2PS_{12}$	4.0	$\text{Li}_{10}\text{SnP}_2\text{S}_{12}$	4.0	119 and 120
$A_4BS_4$	$Na_4SnS_4$	$6.4 \times 10^{-5}$	Li <sub>4</sub> SnS <sub>4</sub>	0.07	11 and 121
$A_4BS_4$	Na <sub>4</sub> SiS <sub>4</sub>	0.02	Li <sub>4</sub> SiS <sub>4</sub>	$9.36 \times 10^{-4}$	122 and 123
$A_3BS_{4-x}Se_x$	Na <sub>3</sub> SbS <sub>3</sub> Se	0.85	Li <sub>3</sub> SbSSe <sub>3</sub>	_	54
$A_3BS_{4-x}Se_x$	$Na_3SbS_{3.75}Se_{0.25}$	4.03	Li <sub>3</sub> SbSSe <sub>3</sub>	_	53
$A_3BS_{4-x}Cl_x$	$Na_{3}SbS_{3.95}Cl_{0.05}$	0.9	$\text{Li}_3\text{SbS}_{4-x}\text{Cl}_x$	_	56
$A_3BS_4$	$Na_{2.88}Sb_{0.88}W_{0.12}S_4$	32.0	$Li_{6.5}Sb_{0.5}Ge_{0.5}S_5I$	16.1	47 and 124
$A_{10+x}B_3S_{12}$	$Na_{10}SnP_2S_{12}$	0.4	$\text{Li}_{10}\text{SnP}_2\text{S}_{12}$	4.0	110, 111, 119 and 120
	Na <sub>10.8</sub> Sn <sub>1.9</sub> PS <sub>11.8</sub>	0.67			
	$Na_{11}Sn_2PS_{12}$	4.0			
$A_3BS_4$	$Na_3P_{0.1}V_{0.9}S_4$	$1.49 \times 10^{-4}$	Li <sub>3</sub> VS <sub>4</sub>	_	125
A <sub>4</sub> SiS <sub>4</sub>	Ga, P co-doping (theoretical) Si, Ta doping (Theoretical)	1.0	Li <sub>4</sub> SiS <sub>4</sub> (Ga, P co-doping) Li <sub>4</sub> SiS <sub>4</sub> (Si, Ta doping)	_	126
	oi, ia doping (incoretical)		Li45154 (51, 1a doping)		

emerging compositions and hybrid strategies reported in recent years. One noteworthy recent example is Sn doping by Zhang et al., which displayed ionic conductivity boosted up to  $\sim$  1.4 mS cm $^{-1}$  by leveraging alternating partially/fully occupied Na sites. 62 Another emerging direction focuses on substituting P and Sb sites entirely as seen in Na<sub>3</sub>VS<sub>4</sub> reported by Kuang et al., 125 which is isostructural to Na<sub>3</sub>PS<sub>4</sub>. Though this pristine material displayed RT ionic conductivity of 1.16 imes10<sup>-5</sup> mS cm<sup>-1</sup>, upon P-doping the conductivity was improved up to  $1.49 \times 10^{-4}$  mS cm<sup>-1</sup> for composition of x = 0.1. Although these values are far lower than an earlier report, it is noteworthy that such sincere attempts pave the way to design the next generation of solid electrolytes for solid-state Na-ion batteries. As technology evolves, new electrolyte materials are discovered and screened using numerous computational efforts, including density functional theory/ab initio molecular dynamics calculations 127-131 and artificial intelligence/machine learning (AI/ML), 132 which have been applied as Na-based superionic conductors (Fig. 5). Among them, a recent report<sup>127</sup> by Ouyang et al. includes ionic conductivity of 48 potential Na-based argyrodites which have been examined for the phase stability and electrochemical stability. However, experimentalists are more curious about well-established Na<sub>4</sub>MS<sub>4</sub> (M = Si, Ga, P, and Ta) than argyrodites, which was reported <sup>126</sup> by Jang et al. in 2024. While promising room-temperature ionic conductivities have already been demonstrated by some sulfide solid electrolytes, the systematic and expansive search for stable Na-M-P-S compounds remains an eminent challenge. In their study, they leveraged a multi-stage DFT workflow with high-throughput screening, geometrical optimization, and ab initio molecular dynamics to discover various metastable/stable compositions with greater than 1 mS cm<sup>-1</sup> at room temperature. These computationally guided approaches enable the systematic exploration and prediction of defect formation, migration energies, and, ultimately, ionic transport mechanisms, thereby substantially accelerating the discovery and optimization of emerging sodium sulfide electrolytes. As a result, the study suggested two parent doping combinations as most promising

such as Ga, P co-doping in Na<sub>4</sub>SiS<sub>4</sub> and Si, Ta doping variants in  $Na_4SiS_4$  (Fig. 4(b)).

### 8. Practical implications and challenges

Since the first use of  $\beta$ -alumina electrolyte for high-temperature sodium-sulfur batteries in the 1960s, numerous efforts over decades have developed diverse types of solid electrolytes to meet the requirement of ASSSBs at RT. Typically, ASSSBs are assembled in a set consisting of a cathode, anode, and solid electrolyte. The key functionality of a solid electrolyte is similar to that of a separator in liquid electrolyte-based sodium batteries. However, for practical applications, the usability is hindered by numerous factors such as weak mechanical stability, low ionic conductivity and poor electrode/electrolyte interfacial compatibility. Conversely, the key properties required for high-performance solid electrolytes at RT are high ionic conductivity, often enabled by engineered defects, alongside good mechanical characteristics, interfacial compatibility and above all high chemical and electrochemical stability. To achieve practical energy densities, these solid electrolyte layers need to be thinner than 50 µm. 133 However, when scaling up for larger formats, the poor mechanical property of inorganic solid electrolytes makes them brittle, posing a greater challenge in processing. In addition, the practical realization of highperformance solid electrolytes must consider doping strategies that enhance defect-mediated ionic transport. Optimized doping not only improves conductivity but also stabilizes specific crystal phases, providing a scalable pathway to tailor electrolyte properties. On the other hand, polymer composites can allow roll-to-roll manufacturing with good elasticity and adhesion to current collectors. For commercial applications, when solution processing is used, the compatibility of solvents and binders with sulfide-based solid electrolytes must be considered. 129 In particular, organic solvents with a polarity index of below 3.1 are fully compatible with sulfide-based solid electrolytes. 130

While these compatibility metrics are well established in lithium-based systems, equivalent systematic investigations tailored to sodium sulfide-based solid electrolytes remain limited and are urgently needed. In addition, for commercialization, the stability of solid electrolytes under ambient conditions needs to be considered. For example, NPS electrolytes can spontaneously undergo hydrolysis when exposed to moisture, producing H<sub>2</sub>S gas and posing a serious safety hazard. To avoid this, solid electrolytes should be used under dry-room conditions, similar to conventional LIBs, which may add to the cost of manufacturing. It is noticeable that many recent reports  $^{47,134,135}$  of the  $\mathrm{Na_3SbS_4}$  family with various doping steps are in line with these moisture requirements and adding additional studies related to H2S exposure in a highly humid environment up to few hours. Computational studies-particularly those focused on defect energetics, ion migration barriers, and phase stability predictions—are becoming indispensable for identifying promising candidates. These techniques should be integrated early in the materials screening process to reduce experimental workload and accelerate scalable materials development. In reality, such exposure data for much longer times such as a few days and even months are required to understand their true capabilities against moisture. With rapid battery adoption, the need for sustainable battery components is of the utmost importance. While it is costlier to redesign at a later stage, future ASSSB manufacturers should consider sustainability as part of the development and manufacturing process.

### 9. Future directions and conclusions

In summary, this review comprehensively explores the defect of chemistry and its implications in ion transport mechanisms of sodium sulfide solid electrolytes. By analyzing intrinsic and extrinsic defects, grain boundary effects, and utilizing advanced computational insights, this study underscores the importance of defect engineering strategies for enhancing ionic conductivity and electrochemical stability of sulfide-based solid electrolytes for Na batteries. The correlation involves a range of factors including synthesis procedure, structural characteristics, and diffusion mechanisms. The comparative analysis between sodium and lithium systems highlights the unique challenges and opportunities presented by sodium solid–electrolyte systems over lithium-based materials.

Despite a leap of achievements such as working temperature from high temperature to room temperature and ionic conductivities from  $10^{-4}~{\rm mS~cm^{-1}}$  to  $>10~{\rm mS~cm^{-1}}$ , several knowledge gaps still prevail in sodium solid electrolytes. To address these, future research should focus on the following key areas:

(1) Interfacial stability: more new strategies should be developed to improve the interfacial stability between sodium metal anodes and sulfide solid electrolytes. This includes exploring new avenues such as alloy-based anodes, surface treatment techniques and possible extensions to anode free systems to prevent detrimental dendrite formation and enhance cycling stability.

- (2) Grain boundary behavior: more deeper investigations into the role of gain boundaries in ion transport and defect segregation is crucial. This can provide insights into the interplay between nano crystallites and grain boundaries, optimizing the microstructure for enhanced performance.
- (3) Defect and doping strategies: continued research into both intrinsic and extrinsic defect engineering, including aliovalent doping, vacancy manipulation, and phase stabilization is crucial for enhancing ionic conductivity. Tailoring dopant type and concentration can significantly impact carrier mobility and phase stability, thereby optimizing electrolyte performance for practical applications.
- (4) Advanced computational and experimental techniques: leveraging advanced techniques such as artificial intelligence (AI) and machine learning (ML) alongside density functional theory (DFT) studies and experimental validations can expedite new materials discovery and refine defect-engineering approaches. To predict and validate these novel compositions with high ionic conductivity and stability, integration of these techniques seamlessly is critical. Increasingly, machine learning (ML) models are expected to play a central role in predicting defect energetics, migration pathways, and phase stability in next-generation solid electrolytes.
- (5) Manufacturability and scalability: currently, there are various practical challenges for commercial application, which require sufficient addressing before scale up. This includes improving compatibility with organic solvents and polymer binders, ensuring the mechanical properties of inorganic solid electrolytes and developing cost-effective manufacturing processes.

By strategically addressing these areas, future research can pave the way for the development of high-performance sulfidebased solid electrolytes and all-solid-state sodium batteries, thereby contributing to a cleaner, safer, and more sustainable energy future.

### Conflicts of interest

There are no conflicts to declare.

## Data availability

No primary research results, software or code have been included and no new data were generated or analyzed as part of this review.

## Acknowledgements

This work was supported by the National Research Foundation of Korea (RS-2024-00454354).

### References

- 1 B. Dunn, H. Kamath and J. M. Tarascon, *Science*, 2011, 334, 928-935.
- 2 J. B. Goodenough and Y. Kim, Chem. Mater., 2010, 22, 587-603.

- 3 T. Arizumi and S. Tani, J. Phys. Soc. Jpn., 1950, 5, 442-447.
- 4 T. Takahashi, K. Kuwabara and M. Shibata, Solid State Ionics, 1980, 1, 163-175.
- 5 M. Tatsumisago and A. Hayashi, Int. J. Appl. Glass Sci., 2014, 5, 226-235.
- 6 A. Sakuda, A. Hayashi and M. Tatsumisago, Sci. Rep., 2013, 3, 2261.
- 7 M. Uematsu, S. Yubuchi, K. Noi, A. Sakuda, A. Hayashi and M. Tatsumisago, Solid State Ionics, 2018, 320, 33-37.
- 8 Q. Zhang, D. Cao, Y. Ma, A. Natan, P. Aurora and H. Zhu, Adv. Mater., 2019, 31(44), 1901131.
- 9 A. Hayashi, K. Noi, A. Sakuda and M. Tatsumisago, Nat. Commun., 2012, 3, 856.
- 10 L. Zhang, K. Yang, J. Mi, L. Lu, L. Zhao, L. Wang, Y. Li and H. Zeng, Adv. Energy Mater., 2015, 5(24), 1501294.
- 11 H. Jia, Y. Sun, Z. Zhang, L. Peng, T. An and J. Xie, Energy Storage Mater., 2019, 23, 508-513.
- 12 A. Nasu, T. Inaoka, F. Tsuji, K. Motohashi, A. Sakuda, M. Tatsumisago and A. Hayashi, ACS Appl. Mater. Interfaces, 2022, 14, 24480-24485.
- 13 X. Guo, S. Halacoglu, Y. Chen and H. Wang, Small, 2024, 20, 2311195.
- 14 I. H. Chu, C. S. Kompella, H. Nguyen, Z. Zhu, S. Hy, Z. Deng, Y. S. Meng and S. P. Ong, Sci. Rep., 2016, 6, 33733.
- 15 T. Fuchs, S. P. Culver, P. Till and W. G. Zeier, ACS Energy Lett., 2020, 5, 146-151.
- 16 T. Krauskopf, S. Muy, S. P. Culver, S. Ohno, O. Delaire, Y. Shao-Horn and W. G. Zeier, J. Am. Chem. Soc., 2018, 140, 14464-14473.
- 17 N. J. J. De Klerk and M. Wagemaker, Chem. Mater., 2016, 28, 3122-3130.
- 18 T. Famprikis, H. Bouyanfif, P. Canepa, M. Zbiri, J. A. Dawson, E. Suard, F. Fauth, H. Y. Playford, D. Dambournet, O. J. Borkiewicz, M. Courty, O. Clemens, J. N. Chotard, M. S. Islam and C. Masquelier, Chem. Mater., 2021, 33, 5652-5667.
- 19 T. Famprikis, J. A. Dawson, F. Fauth, O. Clemens, E. Suard, B. Fleutot, M. Courty, J. N. Chotard, M. S. Islam and C. Masquelier, ACS Mater. Lett., 2019, 1, 641-646.
- 20 H. Nakajima, H. Tsukasaki, J. Ding, T. Kimura, T. Nakano, A. Nasu, A. Hirata, A. Sakuda, A. Hayashi and S. Mori, J. Power Sources, 2021, **511**, 230444.
- 21 C. Yu, S. Ganapathy, N. J. J. De Klerk, E. R. H. Van Eck and M. Wagemaker, J. Mater. Chem. A, 2016, 4, 15095-15105.
- 22 A. Hayashi, K. Noi, N. Tanibata, M. Nagao and M. Tatsumisago, J. Power Sources, 2014, 258, 420-423.
- 23 H. Nguyen, A. Banerjee, X. Wang, D. Tan, E. A. Wu, J.-M. Doux, R. Stephens, G. Verbist and Y. S. Meng, J. Power Sources, 2019, 435, 126623,
- 24 N. Tanibata, K. Noi, A. Hayashi and M. Tatsumisago, RSC Adv., 2014, 4, 17120-17123.
- 25 R. P. Rao, H. Chen, L. L. Wong and S. Adams, J. Mater. Chem. A, 2017, 5, 3377-3388.
- 26 Z. Yu, S. Shang, J. Seo, D. Wang, X. Luo, Q. Huang, S. Chen, J. Lu, X. Li, Z. Liu and D. Wang, Adv. Mater., 2017, 29(16), 1605561.
- 27 F. Tsuji, A. Nasu, A. Sakuda, M. Tatsumisago and A. Hayashi, J. Power Sources, 2021, 506, 230100.
- 28 C. K. Moon, H. J. Lee, K. H. Park, H. Kwak, J. W. Heo, K. Choi, H. Yang, M. S. Kim, S. T. Hong, J. H. Lee and Y. S. Jung, ACS Energy Lett., 2018, 3, 2504-2512.
- 29 X. Feng, P. H. Chien, Z. Zhu, I. H. Chu, P. Wang, M. Immediato-Scuotto, H. Arabzadeh, S. P. Ong and Y. Y. Hu, Adv. Funct. Mater., 2019, **29**(9), 1807951.
- 30 H. Huang, H. H. Wu, X. Wang, B. Huang and T. Y. Zhang, Phys. Chem. Chem. Phys., 2018, 20, 20525-20533.
- M. Uematsu, S. Yubuchi, F. Tsuji, A. Sakuda, A. Hayashi and M. Tatsumisago, J. Power Sources, 2019, 428, 131-135.
- 32 Y. Hibi, N. Tanibata, A. Hayashi and M. Tatsumisago, Solid State Ionics, 2015, 270, 6-9.
- 33 K. H. Park, D. H. Kim, H. Kwak, S. H. Jung, H. J. Lee, A. Banerjee, J. H. Lee and Y. S. Jung, J. Mater. Chem. A, 2018, 6, 17192-17200.
- 34 W. D. Richards, L. J. Miara, Y. Wang, J. C. Kim and G. Ceder, Chem. Mater., 2016, 28, 266-273.
- 35 S. H. Bo, Y. Wang and G. Ceder, J. Mater. Chem. A, 2016, 4, 9044-9053.
- 36 H. Wang, Y. Chen, Z. D. Hood, G. Sahu, A. S. Pandian, J. K. Keum, K. An and C. Liang, Angew. Chem., Int. Ed., 2016, 55, 8551-8555.

37 L. Zhang, D. Zhang, K. Yang, X. Yan, L. Wang, J. Mi, B. Xu and Y. Li, Adv. Sci., 2016, 3(10), 201600089.

- 38 A. Banerjee, K. H. Park, J. W. Heo, Y. J. Nam, C. K. Moon, S. M. Oh, S. T. Hong and Y. S. Jung, Angew. Chem., Int. Ed., 2016, 55, 9634-9638.
- 39 H. Wang, M. Yu, Y. Wang, Z. Feng, Y. Wang, X. Lu, J. Zhu, Y. Ren and C. Liang, J. Power Sources, 2018, 401, 111-116.
- 40 D. Zhang, X. Cao, D. Xu, N. Wang, C. Yu, W. Hu, X. Yan, J. Mi, B. Wen, L. Wang and L. Zhang, Electrochim. Acta, 2018, 259, 100-109.
- 41 S. Halacoglu, S. Chertmanova, Y. Chen, Y. Li, M. Rajapakse, G. Sumanasekera, B. Narayanan and H. Wang, ChemSusChem, 2021, 14, 5161-5166.
- 42 H. Wang, Y. Chen, Z. D. Hood, J. K. Keum, A. S. Pandian, M. Chi, K. An, C. Liang and M. K. Sunkara, ACS Appl. Energy Mater., 2018, 1,
- 43 H. Gamo, N. H. H. Phuc, R. Matsuda, H. Muto and A. Matsuda, Mater. Today Energy, 2019, 13, 45-49.
- 44 Q. Zhang, C. Zhang, Z. D. Hood, M. Chi, C. Liang, N. H. Jalarvo, M. Yu and H. Wang, Chem. Mater., 2020, 32, 2264-2271.
- 45 L. Yu, Q. Jiao, B. Liang, H. Shan, C. Lin, C. Gao, X. Shen and S. Dai, J. Alloys Compd., 2022, 913, 165229.
- 46 J. W. Heo, A. Banerjee, K. H. Park, Y. S. Jung and S. Hong, Adv. Energy Mater., 2018, 8(11), 1702716.
- 47 A. Hayashi, N. Masuzawa, S. Yubuchi, F. Tsuji, C. Hotehama, A. Sakuda and M. Tatsumisago, Nat. Commun., 2019, 10, 5266.
- 48 X. Feng, H. Fang, P. Liu, N. Wu, E. C. Self, L. Yin, P. Wang, X. Li, P. Jena, J. Nanda and D. Mitlin, Angew. Chem., Int. Ed., 2021, 60, 26158-26166.
- 49 T. Famprikis, O. U. Kudu, J. A. Dawson, P. Canepa, F. Fauth, E. Suard, M. Zbiri, D. Dambournet, O. J. Borkiewicz, H. Bouyanfif, S. P. Emge, S. Cretu, J. N. Chotard, C. P. Grey, W. G. Zeier, M. S. Islam and C. Masquelier, J. Am. Chem. Soc., 2020, 142, 18422-18436.
- 50 S. Yubuchi, A. Ito, N. Masuzawa, A. Sakuda, A. Hayashi and M. Tatsumisago, J. Mater. Chem. A, 2020, 8, 1947-1954.
- 51 J. Y. Seo, S. Shim, J. W. Lee, B. Do Lee, S. Park, W. B. Park, S. Han, M. Pyo and K. S. Sohn, J. Mater. Chem. A, 2022, 10, 1831-1839.
- 52 L. Shu, B. Liang, L. Yu, C. Lin, C. Gao, X. Shen, Y. Liu and Q. Jiao, Ceram. Int., 2022, 48, 35134-35140.
- 53 H. Wan, J. P. Mwizerwa, F. Han, W. Weng, J. Yang, C. Wang and X. Yao, Nano Energy, 2019, 66, 104109.
- 54 S. Xiong, Z. Liu, H. Rong, H. Wang, M. McDaniel and H. Chen, Sci. Rep., 2018, 8, 9146.
- 55 S. Yubuchi, A. Hayashi and M. Tatsumisago, Chem. Lett., 2015, 44,
- 56 H. Gamo, N. H. H. Phuc, H. Muto and A. Matsuda, ACS Appl. Energy Mater., 2021, 4, 6125-6134.
- 57 X. Zhang, K. C. Phuah and S. Adams, Chem. Mater., 2021, 33, 9184-9193.
- 58 Y. Tian, T. Shi, W. D. Richards, J. Li, J. C. Kim, S. H. Bo and G. Ceder, Energy Environ. Sci., 2017, 10, 1150-1166.
- 59 V. S. Kandagal, M. D. Bharadwaj and U. V. Waghmare, J. Mater. Chem. A, 2015, 3, 12992-12999.
- 60 S. P. Ong, Y. Mo, W. D. Richards, L. Miara, H. S. Lee and G. Ceder, Energy Environ. Sci., 2012, 6, 148-156.
- 61 Z. Zhu, H. Tang, J. Qi, X. G. Li and S. P. Ong, Adv. Energy Mater., 2021, 11, 2003196.
- 62 Z. Zhang, E. Ramos, F. Lalere, A. Assoud, K. Kaup, P. Hartman and L. F. Nazar, Energy Environ. Sci., 2018, 11, 87-93.
- 63 J. E. Lee, K. Park, J. C. Kim, T. Wi, A. R. Ha, Y. B. Song, D. Y. Oh, J. Woo, S. H. Kweon, S. J. Yeom, W. Cho, K. Kim, H. Lee, S. K. Kwak and Y. S. Jung, Adv. Mater., 2022, 34(16), 2200083.
- 64 M. A. Kraft, L. M. Gronych, T. Famprikis, S. Ohno and W. G. Zeier, Chem. Mater., 2020, 32, 6566-6576.
- 65 E. P. Ramos, Z. Zhang, A. Assoud, K. Kaup, F. Lalere and L. F. Nazar, Chem. Mater., 2018, 30, 7413-7417.
- 66 H. Wan, L. Cai, W. Weng, J. P. Mwizerwa, J. Yang and X. Yao, J. Power Sources, 2020, 449, 227515.
- 67 P. Benedek, N. Yazdani, H. Chen, N. Wenzler, F. Juranyi, M. Månsson, M. S. Islam and V. C. Wood, Sustainable Energy Fuels, 2019. 3. 508-513.
- 68 M. A. Kraft, L. M. Gronych, T. Famprikis and W. G. Zeier, ACS Appl. Energy Mater., 2021, 4, 7250-7258.
- 69 W. Weng, G. Liu, L. Shen and X. Yao, J. Power Sources, 2021, 512, 230485.

- 70 Z. Yu, S. L. Shang, D. Wang, Y. C. Li, H. P. Yennawar, G. Li, H. T. Huang, Y. Gao, T. E. Mallouk, Z. K. Liu and D. Wang, *Energy Storage Mater.*, 2019, 17, 70–77.
- 71 M. Duchardt, S. Neuberger, U. Ruschewitz, T. Krauskopf, W. G. Zeier, J. S. Auf Der Günne, S. Adams, B. Roling and S. Dehnen, *Chem. Mater.*, 2018, 30, 4134–4139.
- 72 F. Han, Y. Zhu, X. He, Y. Mo and C. Wang, Adv. Energy Mater., 2016, 6, 1501590.
- 73 Y. Zhu, X. He and Y. Mo, J. Mater. Chem. A, 2016, 4, 3253-3266.
- 74 Y. Zhu, X. He and Y. Mo, ACS Appl. Mater. Interfaces, 2015, 7, 23685–23693.
- 75 T. An, H. Jia, L. Peng and J. Xia, ACS Appl. Mater. Interfaces, 2020, 12, 20563–20569.
- 76 G. Deysher, Y.-T. Chen, B. Sayahpour, S. Wan-Hsuan Lin, S.-Y. Ham, P. Ridley, A. Cronk, E. A. Wu, D. H. S. Tan, J.-M. Doux, J. An Sam Oh, J. Jang, L. Hoang Bao Nguyen and Y. Shirley Meng, ACS Appl. Mater. Interfaces, 2022, 14, 47715.
- 77 M. Moorthy, R. Thangavel, B. Krishnan Ganesan, A. Saha, S. Hong and Y.-S. Lee, *Chem. Eng. J.*, 2024, **498**, 155234.
- 78 M. Moorthy, B. Moorthy, B. K. Ganesan, A. Saha, S. Yu, D. H. Kim, S. Hong, S. Park, K. Kang, R. Thangavel and Y. S. Lee, *Adv. Funct. Mater.*, 2023, 33(42), 202300135.
- 79 E. A. Wu, C. S. Kompella, Z. Zhu, J. Z. Lee, S. C. Lee, I.-H. Chu, H. Nguyen, S. Ping Ong, A. Banerjee and Y. Shirley Meng, ACS Appl. Mater. Interfaces, 2018, 10, 10076–10086.
- 80 M. Lazar, S. Kmiec, A. Joyce and S. W. Martin, ACS Appl. Energy Mater., 2020, 3, 11559–11569.
- 81 C. Hansel, P. Kumar and D. Kundu, Chem. Mater., 2020, 32(24), 10501.
- 82 L. Li, R. Xu, L. Zhang, Z. Zhang, M. Yang, D. Liu, X. Yan, A. Zhou, L. Li, R. Xu, L. Zhang, Z. Zhang, M. Yang, D. Liu, X. Yan and A. Zhou, Adv. Funct. Mater., 2022, 32(31), 2203095.
- 83 Y. Tian, Y. Sun, D. C. Hannah, Y. Xiao, H. Liu, K. W. Chapman, S. H. Bo and G. Ceder, *Joule*, 2019, 3, 1037–1050.
- 84 S. Zhang, Y. Zhao, F. Zhao, L. Zhang, C. Wang, X. Li, J. Liang, W. Li, Q. Sun, C. Yu, J. Luo, K. Doyle-Davis, R. Li, T.-K. Sham and X. Sun, Adv. Funct. Mater., 2022, 30(22), 2001118.
- 85 Y. Zhao, J. Liang, Q. Sun, L. V. Goncharova, J. Wang, C. Wang, K. R. Adair, X. Li, F. Zhao, Y. Sun, R. Li and X. Sun, J. Mater. Chem. A, 2019, 7, 4119–4125.
- 86 Y. Li, S. Halacoglu, V. Shreyas, W. Arnold and X. Guo, *Chem. Eng. J.*, 2022, 434, 134679.
- 87 Y. Li, W. Arnold, S. Halacoglu, J. B. Jasinski, T. Druffel, H. Wang, Y. Li, W. Arnold, S. Halacoglu, H. Wang, J. B. Jasinski and T. Druffel, Adv. Funct. Mater., 2021, 31(28), 2101636.
- 88 A. Kuhn, V. Duppel and B. V. Lotsch, Energy Environ. Sci., 2013, 6, 3548-3552.
- 89 T. Krauskopf, S. P. Culver and W. G. Zeier, *Inorg. Chem.*, 2018, 57, 4739–4744
- M. Duchardt, U. Ruschewitz, S. Adams, S. Dehnen and B. Roling, *Angew. Chem., Int. Ed.*, 2018, 57, 1351–1355.
- 91 R. Raj and J. Wolfenstine, J. Power Sources, 2017, 343, 119-126.
- 92 F. Shen, M. B. Dixit, X. Xiao and K. B. Hatzell, ACS Energy Lett., 2018, 3, 1056–1061.
- S. Stegmaier, J. Voss, K. Reuter and A. C. Luntz, *Chem. Mater.*, 2017, 29, 4330–4340.
- 94 L. Porz, T. Swamy, B. W. Sheldon, D. Rettenwander, T. Fromling, H. L. Thaman, S. Berendts, R. Uecker, W. Craig Carter and Y.-M. Chiang, Adv. Energy Mater., 2017, 7, 1701003.
- 95 Z. Liu, W. Fu, E. A. Payzant, X. Yu, Z. Wu, N. J. Dudney, J. Kiggans, K. Hong, A. J. Rondinone and C. Liang, J. Am. Chem. Soc., 2013, 135, 975–978.
- 96 H. Tsukasaki, S. Mori, H. Morimoto, A. Hayashi and M. Tatsumisago, Sci. Rep., 2017, 7, 1–7.
- 97 P. Bron, S. Dehnen and B. Roling, J. Power Sources, 2016, 329, 530-535.
- 98 Y. Sun, K. Suzuki, S. Hori, M. Hirayama and R. Kanno, *Chem. Mater.*, 2017, **29**, 5858–5864.
- 99 P. Padma Kumar and S. Yashonath, J. Chem. Sci., 2006, 118, 135-154.
- 100 Z. Zhu, I. H. Chu, Z. Deng and S. P. Ong, Chem. Mater., 2015, 27, 8318–8325.
- 101 M. K. Gupta, J. Ding, N. C. Osti, D. L. Abernathy, W. Arnold, H. Wang, Z. Hood and O. Delaire, *Energy Environ. Sci.*, 2021, 14, 6554–6563.
- 102 F. Han, J. Yue, X. Fan, T. Gao, C. Luo, Z. Ma, L. Suo and C. Wang, Nano Lett., 2016, 16, 4521–4527.

103 I. H. Chu, C. S. Kompella, H. Nguyen, Z. Zhu, S. Hy, Z. Deng, Y. S. Meng and S. P. Ong, *Sci. Rep.*, 2016, 6, 1–10.

- 104 J. A. Dawson, P. Canepa, M. J. Clarke, T. Famprikis, D. Ghosh and M. S. Islam, *Chem. Mater.*, 2019, 31, 5296–5304.
- 105 L. Yang, S. Geng, Y. He, X. Ming and X. Kuang, *J. Phys. Chem. C*, 2022, **126**, 6161–6170.
- 106 Y. Kato, S. Hori, T. Saito, K. Suzuki, M. Hirayama, A. Mitsui, M. Yonemura, H. Iba and R. Kanno, *Nat. Energy*, 2016, 1, 16030.
- 107 H. Wang, Y. Chen, Z. D. Hood, G. Sahu, A. S. Pandian, J. K. Keum, K. An and C. Liang, *Angew. Chem., Int. Ed.*, 2016, 55, 8551–8555.
- 108 L. E. Rush, Z. D. Hood and N. A. W. Holzwarth, Phys. Rev. Mater., 2017, 1, 75405.
- 109 R. Jalem, A. Hayashi, F. Tsuji, A. Sakuda and Y. Tateyama, *Chem. Mater.*, 2020, 32, 8373–8381.
- 110 W. D. Richards, T. Tsujimura, L. J. Miara, Y. Wang, J. C. Kim, S. P. Ong, I. Uechi, N. Suzuki and G. Ceder, *Nat. Commun.*, 2016, 7, 11009.
- 111 Z. Yu, S. L. Shang, Y. Gao, D. Wang, X. Li, Z. K. Liu and D. Wang, Nano Energy, 2018, 47, 325–330.
- 112 S. H. Bo, Y. Wang, J. C. Kim, W. D. Richards and G. Ceder, *Chem. Mater.*, 2016, 28, 252–258.
- 113 N. Kamaya, K. Homma, Y. Yamakawa, M. Hirayama, R. Kanno, M. Yonemura, T. Kamiyama, Y. Kato, S. Hama, K. Kawamoto and A. Mitsui, *Nat. Mater.*, 2011, **10**, 682–686.
- 114 J. Kim, Y. Yoon, M. Eom and D. Shin, Solid State Ionics, 2012, 225, 626–630.
- 115 S. P. Ong, W. D. Richards, A. Jain, G. Hautier, M. Kocher, S. Cholia, D. Gunter, V. L. Chevrier, K. A. Persson and G. Ceder, *Comput. Mater. Sci.*, 2013, 68, 314–319.
- 116 H. Wan, L. Cai, W. Weng, J. P. Mwizerwa, J. Yang and X. Yao, J. Power Sources, 2020, 449, 227515.
- 117 Z. Liu, W. Fu, E. A. Payzant, X. Yu, Z. Wu, N. J. Dudney, J. Kiggans, K. Hong, A. J. Rondinone and C. Liang, *J. Am. Chem. Soc.*, 2013, 135, 975–978.
- 118 T. Kimura, A. Kato, C. Hotehama, A. Sakuda, A. Hayashi and M. Tatsumisago, *Solid State Ionics*, 2019, **333**, 45–49.
- 119 M. Duchardt, U. Ruschewitz, S. Adams, S. Dehnen and B. Roling, Angew. Chem., Int. Ed., 2018, 57, 1351–1355.
- 120 P. Bron, S. Johansson, K. Zick, J. S. A. Der Günne, S. Dehnen and B. Roling, J. Am. Chem. Soc., 2013, 135, 15694–15697.
- 121 G. Sahu, Z. Lin, J. Li, Z. Liu, N. Dudney and C. Liang, *Energy Environ. Sci.*, 2014, 7, 1053–1058.
- 122 N. Tanibata, K. Noi, A. Hayashi and M. Tatsumisago, RSC Adv., 2014, 4, 17120–17123.
- 123 J. Roh, H. Kim, H. Lee, H. Bu, A. Manjon-Sanz, H. Kim and S. T. Hong, *Chem. Mater.*, 2024, **36**, 6973–6984.
- 124 Y. Lee, J. Jeong, H. J. Lee, M. Kim, D. Han, H. Kim, J. M. Yuk, K. W. Nam, K. Y. Chung, H. G. Jung and S. Yu, ACS Energy Lett., 2022, 7, 171–179.
- 125 Y. He, F. Lu and X. Kuang, RSC Adv., 2019, 9, 39180-39186.
- 126 S. H. Jang, R. Jalem and Y. Tateyama, J. Mater. Chem. A, 2024, 12, 20879–20886.
- 127 B. Ouyang, Y. Wang, Y. Sun and G. Ceder, *Chem. Mater.*, 2020, 32, 1896–1903.
- 128 Y. Zhu, X. He and Y. Mo, ACS Appl. Mater. Interfaces, 2015, 7, 23685-23693.
- 129 K. Yang, D. Liu, Z. Qian, D. Jiang and R. Wang, *ACS Nano*, 2021, **15**, 17232–17246.
- 130 H. Kwak, S. Wang, J. Park, Y. Liu, K. T. Kim, Y. Choi, Y. Mo and Y. S. Jung, ACS Energy Lett., 2022, 7, 1776–1805.
- 131 T. Famprikis, J. A. Dawson, F. Fauth, E. Suard, B. Fleutot, M. Courty, J.-N. Chotard, M. Saiful Islam and C. Masquelier, ChemRxiv, 2019, preprint, DOI: 10.26434/CHEMRXIV.8003717.V1.
- 132 S. Shim, W. B. Park, J. Han, J. Lee, B. Do Lee, J. W. Lee, J. Y. Seo, S. J. R. Prabakar, S. C. Han, S. P. Singh, C. C. Hwang, D. Ahn, S. Han, K. Park, K. S. Sohn and M. Pyo, Adv. Sci., 2022, 9, 2201648.
- 133 D. H. S. Tan, A. Banerjee, Z. Chen and Y. S. Meng, *Nat. Nanotechnol.*, 2020, 15, 170–180.
- 134 Y. Zhu, Y. Mo, Y. Zhu and Y. Mo, Angew. Chem., Int. Ed., 2020, 59, 17472–17476.
- 135 Y. Guo, K. Liu, C. Li, D. Song, H. Zhang, Z. Wang, Y. Yan, L. Zhang, S. Dai, Y. Guo, K. Liu, D. Song, H. Zhang, Y. Yan, L. Zhang, C. Li, Z. Wang and S. Dai, Adv. Energy Mater., 2024, 14, 2401504.